2013-06

H-bridge inverter loading analysis for an Energy Management System

Metzcus, Andrew James

Monterey, California: Naval Postgraduate School

NAVAL POSTGRADUATE SCHOOL

MONTEREY, CALIFORNIA

THESIS

H-BRIDGE INVERTER LOADING ANALYSIS FOR AN ENERGY MANAGEMENT SYSTEM

by

Andrew James Metzcus

June 2013

Thesis Advisor: Giovanna Oriti
Co-Advisor: Alexander L. Julian

Approved for public release; distribution is unlimited

THIS PAGE INTENTIONALLY LEFT BLANK

REPORT DOCUMENTATION PAGE			Form Approved OMB No. 0704-0188
Public reporting burden for this collection of information is estimated to average 1 hour per response, including the time for reviewing instruction, searching existing data sources, gathering and maintaining the data needed, and completing and reviewing the collection of information. Send comments regarding this burden estimate or any other aspect of this collection of information, including suggestions for reducing this burden, to Washington headquarters Services, Directorate for Information Operations and Reports, 1215 Jefferson Davis Highway, Suite 1204, Arlington, VA 22202-4302, and to the Office of Management and Budget, Paperwork Reduction Project (0704-0188) Washington DC 20503.			
1. AGENCY USE ONLY *(Leave blank)*	**2. REPORT DATE** June 2013	**3. REPORT TYPE AND DATES COVERED** Master's Thesis	
4. TITLE AND SUBTITLE H-BRIDGE INVERTER LOADING ANALYSIS FOR AN ENERGY MANAGEMENT SYSTEM		**5. FUNDING NUMBERS**	
6. AUTHOR(S) Andrew James Metzcus			
7. PERFORMING ORGANIZATION NAME(S) AND ADDRESS(ES) Naval Postgraduate School Monterey, CA 93943-5000		**8. PERFORMING ORGANIZATION REPORT NUMBER**	
9. SPONSORING /MONITORING AGENCY NAME(S) AND ADDRESS(ES) N/A		**10. SPONSORING/MONITORING AGENCY REPORT NUMBER**	
11. SUPPLEMENTARY NOTES The views expressed in this thesis are those of the author and do not reflect the official policy or position of the Department of Defense or the U.S. Government. IRB Protocol number ____N/A____.			
12a. DISTRIBUTION / AVAILABILITY STATEMENT Approved for public release; distribution is unlimited		**12b. DISTRIBUTION CODE**	

13. ABSTRACT (maximum 200 words)

The Department of the Navy (DON) is committed to reduce its reliance on fossil fuels. Secretary of the Navy Ray Mabus has said, "The underlying reasons for reform are clear. Our energy sources are not secure, we need to be more efficient in energy use, and we emit too much carbon." Microgrids utilizing an Energy Management System (EMS) may be the answer to control and route power more efficiently. The power quality achieved from a single phase pulse-width modulation (PWM) voltage source inverter (VSI) (the "heart" of an EMS) driving an inductive and capacitive (LC) filter with linear and non-linear loads was investigated in this thesis. The open loop PWM waveforms are compared to the power quality standards for ship board power, MIL-STD-1399-300B. This quantifies the performance limits of open loop PWM, which is the simplest control strategy for a single-phase VSI. Closed loop control is shown to be necessary when larger loads are connected to the VSI in order to prevent output voltage sag.

14. SUBJECT TERMS Energy Management System, microgrid			**15. NUMBER OF PAGES** 75
			16. PRICE CODE
17. SECURITY CLASSIFICATION OF REPORT Unclassified	**18. SECURITY CLASSIFICATION OF THIS PAGE** Unclassified	**19. SECURITY CLASSIFICATION OF ABSTRACT** Unclassified	**20. LIMITATION OF ABSTRACT** UU

NSN 7540-01-280-5500

Standard Form 298 (Rev. 2-89)
Prescribed by ANSI Std. 239-18

THIS PAGE INTENTIONALLY LEFT BLANK

Approved for public release; distribution is unlimited

H-BRIDGE INVERTER LOADING ANALYSIS FOR AN ENERGY MANAGEMENT SYSTEM

Andrew James Metzcus
Lieutenant, United States Navy
B.S., Oregon State University, 2006

Submitted in partial fulfillment of the
requirements for the degree of

MASTER OF SCIENCE IN ELECTRICAL ENGINEERING

from the

NAVAL POSTGRADUATE SCHOOL
June 2013

Author: Andrew James Metzcus

Approved by: Giovanna Oriti
Thesis Advisor

Alexander L. Julian
Thesis Co-Advisor

R. Clark Robertson
Chair, Department of Electrical and Computer Engineering

THIS PAGE INTENTIONALLY LEFT BLANK

ABSTRACT

The Department of the Navy (DON) is committed to reduce its reliance on fossil fuels. Secretary of the Navy Ray Mabus has said, "The underlying reasons for reform are clear. Our energy sources are not secure, we need to be more efficient in energy use, and we emit too much carbon." Microgrids utilizing an Energy Management System (EMS) may be the answer to control and route power more efficiently. The power quality achieved from a single phase pulse-width modulation (PWM) voltage source inverter (VSI) (the "heart" of an EMS) driving an inductive and capacitive (LC) filter with linear and non-linear loads was investigated in this thesis. The open loop PWM waveforms are compared to the power quality standards for ship board power, MIL-STD-1399-300B. This quantifies the performance limits of open loop PWM, which is the simplest control strategy for a single-phase VSI. Closed loop control is shown to be necessary when larger loads are connected to the VSI in order to prevent output voltage sag.

THIS PAGE INTENTIONALLY LEFT BLANK

TABLE OF CONTENTS

THIS PAGE INTENTIONALLY LEFT BLANK

LIST OF FIGURES

LIST OF ACRONYMS AND ABBREVIATIONS

AC	Alternating Current
DC	Direct Current
DG	Distributed Generation
DON	Department of the Navy
EMS	Energy Management System
FPGA	Field Programmable Gate Array
IGBT	Insulated Gate Bipolar Transistor
JTAG	Joint Test Action Group
PC	Personal Computer
PCB	Printed Circuit Board
PFC	Power Factor Correction
PWM	Pulse Width Modulation
THD	Total Harmonic Distortion
USB	Universal Serial Bus
VSI	Voltage Source Inverter

THIS PAGE INTENTIONALLY LEFT BLANK

EXECUTIVE SUMMARY

Energy reduction and energy efficiency are two of the top priorities among senior Navy leadership and have been for several years. In October 2009, the Honorable Ray Mabus, Secretary of the Navy, displayed his vision in [1]. He stated, "Reforming energy use and policy within the Department of the Navy will assure the long-term energy security of the United States, encourage development of efficiencies, and promote environmental stewardship. In doing so, we will improve the combat and operational effectiveness of our Forces and maintain our position as the finest Navy and Marine Corps in the world." Currently, the Department of the Navy's (DON) goals are listed in [2] to include a 50% ashore energy consumption reduction by 2020, the call for a the DON to produce at least 50% of shore-based energy requirements from alternative sources by 2020, for half of all DON installations to have a net-zero energy consumption by 2020, and for a 50% reduction of fuel in the commercial vehicle fleet by 2015. As the DON moves forward with an energy savings plan, Energy Management Systems (EMS) will be part of the solution. In [3], an EMS is defined as the interface between the main power grid and a micro grid which includes energy storage and potentially one or more renewable energy sources. An EMS optimizes energy sources and energy storage systems in microgrids in several ways [3]. A microgrid is a small power system compared to that of the main power grid [4] and includes one or more distributed generation (DG) sources. DG systems can be based on renewable energy sources such as batteries, fuel cells, photovoltaic cells, and wind turbines in addition to traditional generators. Figure 1 is an illustration of a microgrid that shows how a photovoltaic cell, awind turbine, two microturbines, and a fuel cell could be arranged. This microgrid can be connected to the main grid through the use of power electronics. The Energy Manager/Controller depicted in Figure 1 is what is referred to in this thesis as the EMS. The EMS monitors all power aspects of both sides of the separation devices for system protection and power quality in order to maintain reliable power to desired loads. DG sources are typically DC or their output is AC but does not meet the main grid's magnitude, frequency and phase requirements [4]; therefore, an inverter is needed to condition the power.

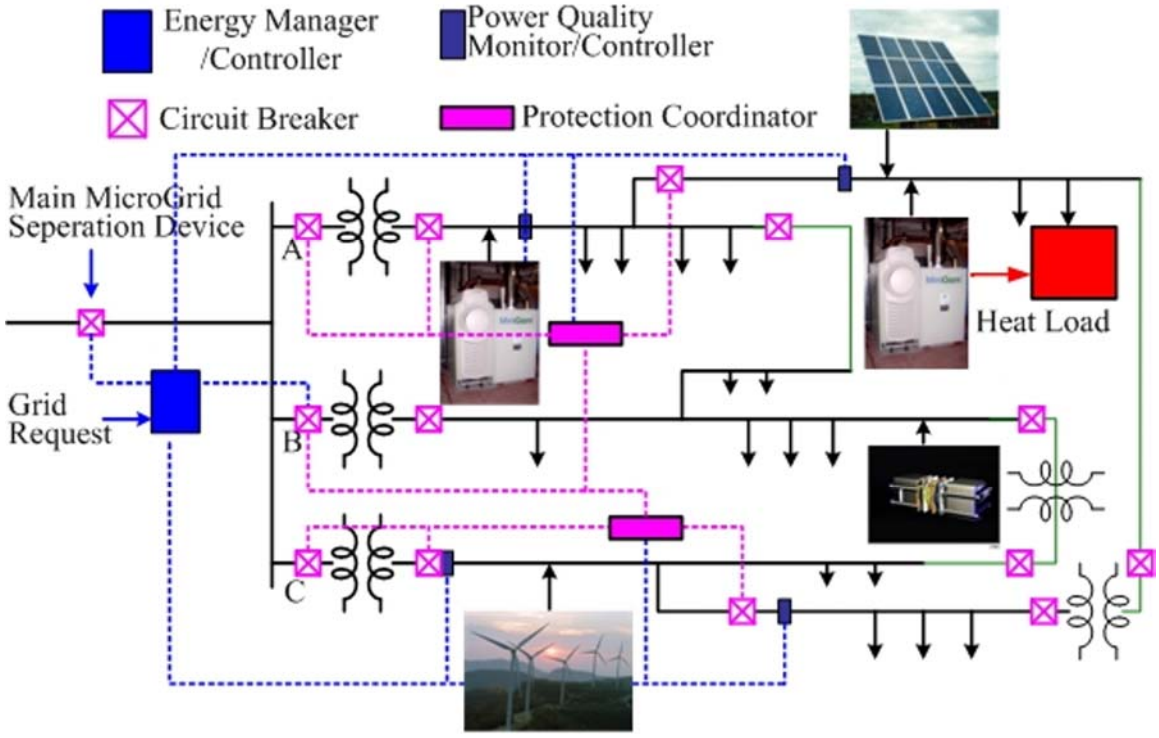

Figure 1. Microgrid system configuration and main features. From [4].
Note: "Separation" is misspelled in cited document.

The objective of this thesis is to evaluate a linear load and a passive diode rectifier load against MIL-STD-1399-300B when connected to a DC supply through a single-phase H-bridge inverter. MIL-STD-1399-300B scopes out the electrical interface characteristics for shipboard equipment utilizing AC electric power.

The approach was to first develop a physics-based model utilizing Simulink and MATLAB. An EMS was then built and tested in the lab which was compared to the model. Once validated, the model could then be used to explore power quality improvement strategies and be further used in the development of optional configurations of the EMS.

In the design of the voltage source inverter (VSI), a switching scheme had to be chosen. In [5], it was stated that unipolar pulse-width modulation (PWM) switching effectively doubled the switching frequency of the inverter when compared to that of bipolar switching. This was validated in the model and the lab. Bipolar switching resulted in more "noise" in the current waveform and higher voltage harmonics near the

switching frequency. Therefore, unipolar switching was deemed the best switching scheme for both loads with respect to MIL-STD-1399-300B.

Analysis and comparison of the diode rectifier load in the model and lab showed that open-loop control would not meet the sinusoidal source specifications of MIL-STD-1399-300B. Active filtering techniques were researched. In [6], analysis of an active filter showed it was very difficult to wave shape the voltage for this load. Furthermore, higher currents are realized in the diodes with a shorter conduction angle when connected with an active filter. This was confirmed by use of the physics-based model.

Analysis and comparison of the linear load in the model and lab showed that open loop control would meet the source specifications of MIL-STD-1399-300B for a linear load. A dynamic linear load would require the use of a simple closed loop proportional and integral (PI) control to account for voltage sagging. The linear load did not pass MIL-STD-1399-300B load harmonic line current specifications due to an out of specification condition near the switching frequency of the VSI. Due to the ideal nature of a resistive load, it was determined that this was due to the non-ideal voltage produced from the VSI even though the source was well within MIL-STD-1399-300B specification.

In conclusion, it was found that MIL-STD-1399-300B has much tighter specifications on loads than it does on power sources. It appears that specifications are slowly being updated to account for advances in newer technology. As shipboard power and industry move to renewable or DC power systems, VSIs will be part of this technological step. A power source that is within specifications should be able to supply power to an ideal source (linear load) while maintaining line currents within specification. A review of VSIs as a power source compared to existing specifications is warranted.

LIST OF REFERENCES

[1] Office of Naval Research. (2009 October). *Naval energy—A strategic approach* [Online]. Available: http://www.onr.navy.mil/naval-energy-forum/~/media/Files/Conferences/Naval%20Energy%20Forum/Naval%20Energy%20Strategy%20overview.ashx

[2] Shore Energy Management, OPNAVINST 4100.5E, June 22, 2012.

[3] G. Oriti, A. L. Julian, and N.J. Peck, "Power electronics enabled energy management systems," in *Proc. of IEEE Applied Power Electronics Conf. (APEC)*, Long Beach, CA, Mar. 2013.

[4] F.Z. Peng, Y.W. Li, and L.M. Tolbert, "Control and protection of power electronics interfaced distributed generation systems in a customer-driven microgrid," in *Proc. of IEEE Power and Energy Society General Meeting*, Calgary, AB, Canada, pp. 1–8, July 2009.

[5] N. Mohan and T. Undeland, W. P. Robbins, Power Electronics, Converters Applications and Design (3rd ed.), New York: John Wiley and Sons, 2003.

[6] J.G. Pinto, P. Neves, R. Pregitzer, L.F. C. Monteiro, and J. L. Afonso, "Single-Phase Shunt Active Filter with Digital Control," in *International Conf. on Renewable Energies and Power Quality (ICREPQ'07),* Seville, Spain, March 2007.

ACKNOWLEDGMENTS

First and foremost, I would like to thank my wife, Yvonne, and my children, Andrew and Lilly, for their support and understanding throughout my studies. Your love and patience during the stressful times helped me more than you'll ever know. You will always have my heart. I love you all.

I would like to thank my parents, Donald and Rita Metzcus, for their continued support and for always believing in me. You have made me who I am, and I will be forever grateful. I love you both.

Last, I would like to thank Dr. Giovanna Oriti and Dr. Alexander Julian for their direction and guidance. As the research pulled me in many directions, your ability to help me focus on the ultimate goal of my thesis was most appreciated. I learned a great deal from both of you that I will take with me throughout my career. It was a pleasure sitting through your classes, and conducting research together. Thank you.

THIS PAGE INTENTIONALLY LEFT BLANK

I. INTRODUCTION

Energy reduction and energy efficiency are two of the top priorities among senior Navy leadership, and has been for several years. In October 2009, the Honorable Ray Mabus, Secretary of the Navy, displayed his vision in [1]. He stated, "Reforming energy use and policy within the Department of the Navy will assure the long-term energy security of the United States, encourage development of efficiencies, and promote environmental stewardship. In doing so, we will improve the combat and operational effectiveness of our Forces and maintain our position as the finest Navy and Marine Corps in the world." Currently, the Department of the Navy's (DON) goals are listed in [2] to include a 50% ashore energy consumption reduction by 2020, the call for a the DON to produce at least 50% of shore-based energy requirements from alternative sources by 2020, for half of all DON installations to have a net-zero energy consumption by 2020, and for a 50% reduction of fuel in the commercial vehicle fleet by 2015.

As the DON moves forward with an energy savings plan, Energy Management Systems (EMS) will be part of the solution. In [3], an EMS is defined as the interface between the main power grid and a micro grid which includes energy storage and potentially one or more renewable energy sources. The additional inherent feature of combining the two grids results in a fault tolerant system that is able to maintain critical loads during a loss to the main grid. This additional feature is a listed policy in [2].

A. OBJECTIVE

The objective of this thesis is to investigate the power quality on a microgrid operating in islanding mode where an EMS is used to interface with and disconnect from the main grid. The EMS includes a single-phase pulse-width modulation (PWM) voltage source inverter (VSI) driving an inductive and capacitive (LC) filter that synthesizes 120 V, 60 Hz voltage for the linear and non-linear loads connected to the microgrid. The open loop PWM waveforms are compared to the power quality standards for ship board power, MIL-STD-1399-300B. This quantifies the performance limits of open loop

PWM, which is the simplest control strategy for a single phase VSI. Closed loop control is shown to be necessary when larger loads are connected to the VSI.

B. APPROACH

In order to accomplish the stated objectives, a physics-based model of the system was developed in MATLAB/Simulink. The system was also implemented in hardware in the lab to validate the Simulink model. Experimental and simulated plots where compared to each other and to MIL-STD-1399-300B limits. Finally, the validated Simulink model was used to study the power quality of the microgrid with different loads. The appendix contains MATLAB code used to process and display the collected data seen throughout this thesis.

II. ENERGY MANAGEMENT SYSTEM BASICS

People today are familiar with the electrical power grid. It is used for almost all day-to-day activities and operations. It is the "heart" of an industrial nation that is dependent on reliable power. As the demand and cost for power increases, the focus on renewable energy and energy efficiency increases. An EMS optimizes energy sources and energy storage systems in microgrids in several ways [3]. A microgrid is a small power system compared to that of the main power grid [4]. It includes one or more distributed generation (DG) sources. DG systems can be based on renewable energy sources such as batteries, fuel cells, photovoltaic cells, and wind turbines. Figure 1 is an illustration of a microgrid that shows how a photovoltaic cell, wind turbine, two microturbines, and a fuel cell could be arranged. This microgrid can be connected to the main grid through the use of power electronics. The Energy Manager/Controller depicted is referred to as the EMS in this thesis. The EMS monitors all power aspects of both sides of the separation devices for system protection and power quality in order to maintain reliable power to desired loads. DG sources are typically DC or their output is AC that does not meet the main grid's magnitude, frequency and phase requirements [4]. Therefore, an inverter is used to convert DC-AC as illustrated in Figure 2. A DC supply is boosted and then converted to AC through pulse-width modulation (PWM), filtered, and then delivered to the load. If the source is non-utility grade AC, it is first rectified by an AC-DC converter. The direct output of a wind turbine is a typical example of non-utility grade AC that must first be converted to DC and then converted to AC to meet utility grade specifications.

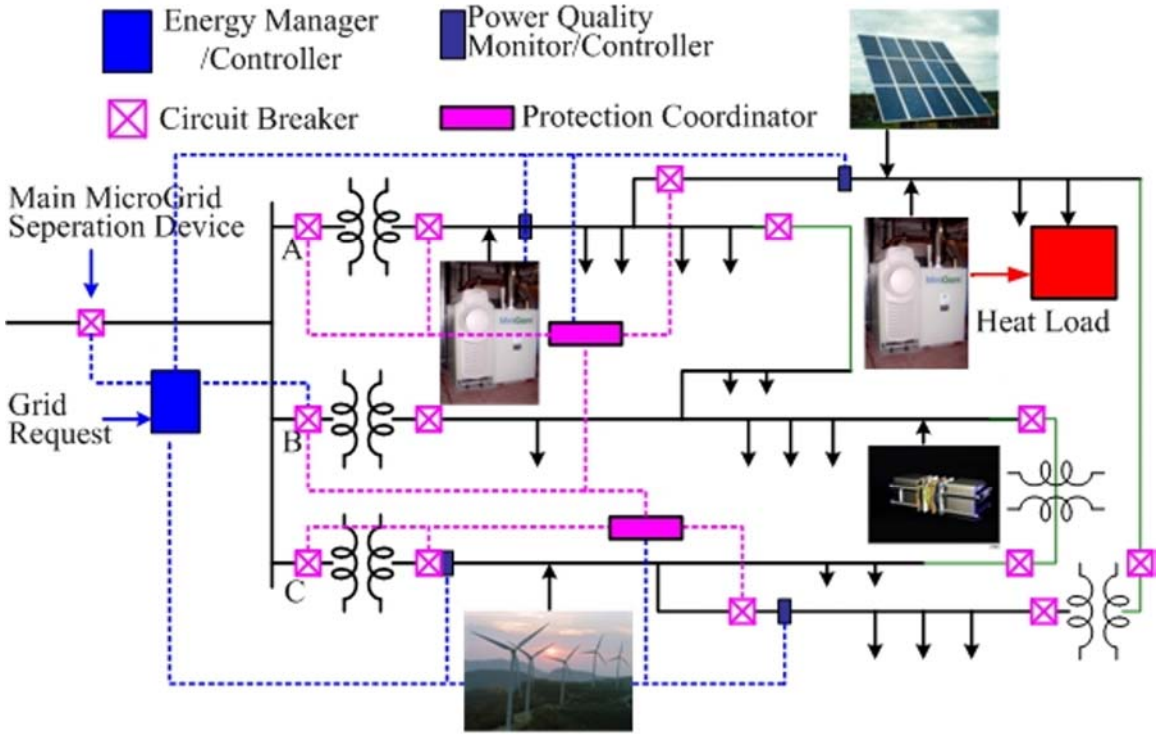

Figure 1. Microgrid system configuration and main features. From [4]. Note: "Separation" is misspelled in cited document.

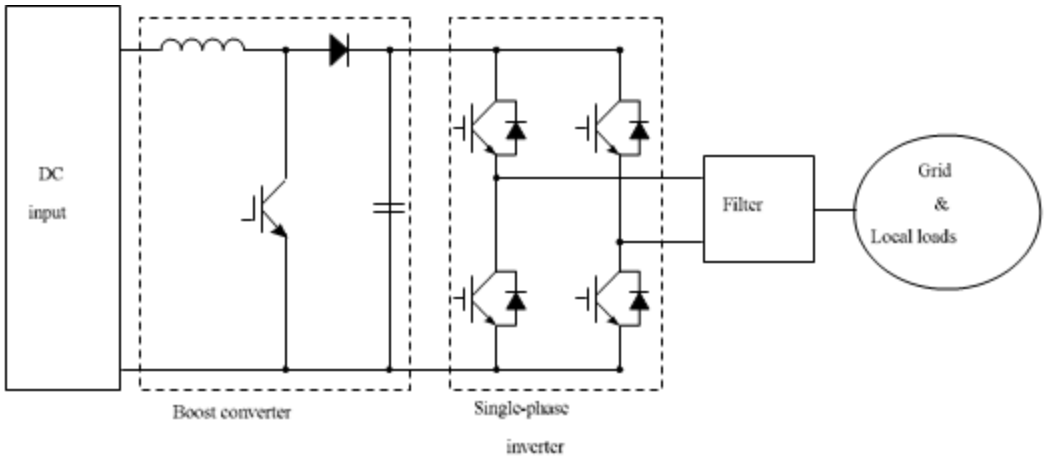

Figure 2. Two-stage DC-AC conversion system with a boost DC-DC converter and a buck DC-AC inverter. From [4].

There are three scenarios illustrated in Figure 3 that show how an EMS can provide reliable power and possibly reduce operating costs [3]. In scenario 1, the EMS system augments power during high power demand periods from the DC energy source

by operating as a current source [3]. This is especially useful in areas that charge higher rates for power used during peak power periods. An example of this would be to charge a battery storage system at night when power rates are lower and then discharge them through the EMS system to augment high power demand during times when power rates are higher. In scenario 2, the EMS system is operating in islanding mode. This allows for maintaining power to vital loads during a loss of main power [3]. The focus of this thesis is the evaluation of the power quality delivered by the EMS hardware and physics-based simulation in this scenario. In scenario 3, peak power is limited by shedding non-critical loads [3]. Where scenario 1 augments the power to keep the total power drawn from the main grid lower, scenario 2 drops non-critical loads as peak power increases. This can easily be accomplished by monitoring incoming power. Another option is an electronic interlock that sheds non-critical loads prior to starting larger loads to keep peak power below a specified threshold or by not allowing large loads to start until total power is below a specified threshold. The use of power electronics allows for almost limitless design and flexibility.

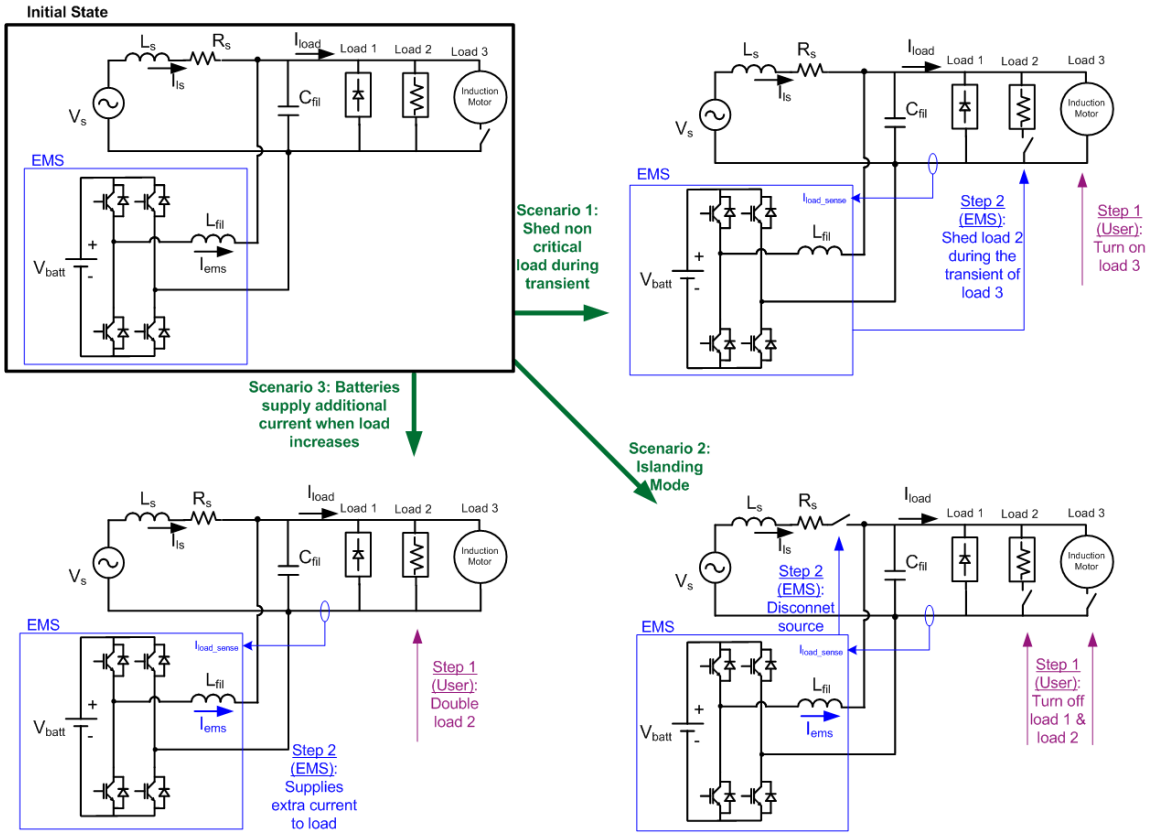

Figure 3. Scenarios used to demonstrate EMS functionality. From [3].

III. HARDWARE DESIGN ELEMENTS AND THEORY

A. FIELD PROGRAMMABLE GATE ARRAY (FPGA)

FPGAs are devices that are said to be field-programmable. That is, they can be programmed in place without removing the component [5], an option that is highly desirable for upgrading a system or utilizing one system for multiple uses. This approach of circuit design can result in monetary savings over a designed system's life. FPGAs were invented in 1984 and are extremely helpful today in the design of electronic devices. This feature was useful in the building of the EMS system, as it allowed changes to the design logic and performance parameters without the need to build new boards at the expense of cost and additional man-hours. FPGAs are semiconductor devices that contain programmable logic components. Software used to program the FPGA connects these logic blocks internally to perform some of the simplest operations to the most complex. XLINX's ISE Design Suite software allowed for the use of Simulink and MATLAB to design the functional architecture and then compile the high level design down to VHDL in order to program the designed functions to the FPGA.

B. INSULATED GATE BIPOLAR TRANSISTOR (IGBT)

IGBTs are power switching semiconductor devices that require only small amounts of energy to switch the device [6]. Their turn-on and turn-off times are approximately 1 μs with voltage ratings up to 6,500 V. Because of this, IGBTs are generally favored for high voltage, high current, and low switching frequencies seen in most power electronics.

A three-leg IGBT power module was used to construct the H-bridge inverter in the EMS. The basic circuit design built is depicted in Figure 2. Four of the six IGBTs on the module form the H-bridge, one was used in the boost converter, and the last IGBT is not used.

C. INVERTER THEORY

An inverter converts a DC source to a desired AC source. The overall objective of an inverter is to control output voltage amplitude and frequency. Designs of inverters have varying degrees of desired outputs from the simplest form of a square wave to more complex sinusoidal output waveforms. The desired output of a single-phase, full-bridge inverter is constructed by controlling the switches shown in Figure 4.

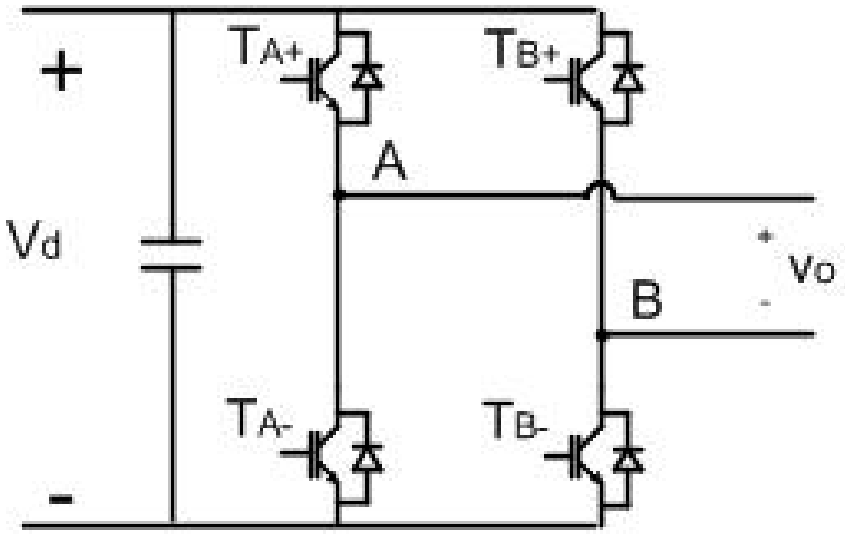

Figure 4. Basic H-bridge inverter.

1. Sine-pulse Width Modulation: BIPOLAR Switching.

This switching scheme treats switches (T_{A+} , T_{B-}) and (T_{A-} , T_{B+}) in Figure 4 as switched pairs. That is, when switches (T_{A+} , T_{B-}) are on, switches (T_{A-} , T_{B+}) are off and vice versa. To determine the switching sequence, a sinusoidal reference signal $v_{control}$ is overlaid on top of a constant triangle wave v_{tri} as shown in Figure 5. The triangle shaped waveform v_{tri} is the carrier waveform, and its frequency is the inverter switching frequency f_s, also called the carrier frequency. The magnitude of v_{tri} and the frequency of f_s are generally kept constant. The waveform $v_{control}$ has a frequency f_1, which is the desired fundamental output frequency of the inverter.

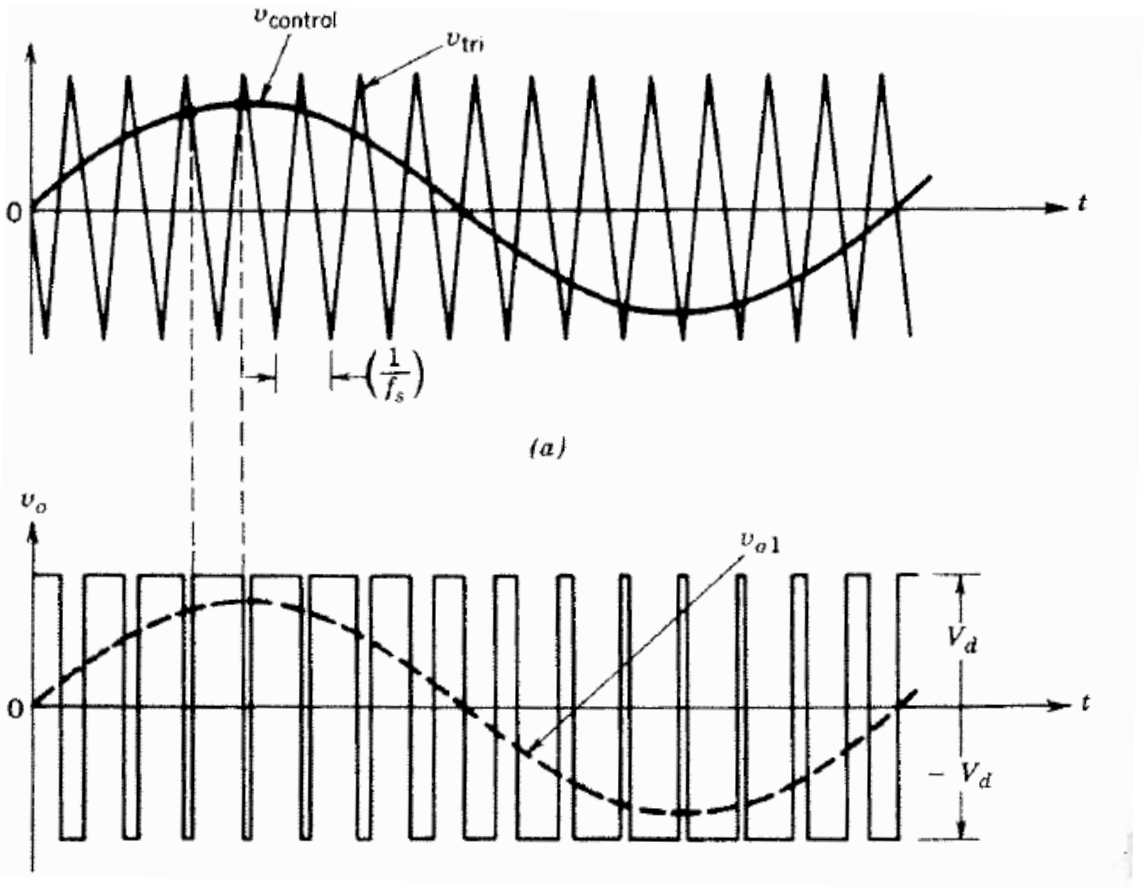

Figure 5. PWM with bipolar voltage switching. From [6].

The switches operate as follows [6]:

$$v_{control} > v_{tri}, \quad T_{A+} \text{ is on, } T_{B-} \text{ is on,} \quad v_o = +V_d \tag{1}$$

$$v_{tri} > v_{control}, \quad T_{A-} \text{ is on, } T_{B+} \text{ is on,} \quad v_o = -V_d \tag{2}$$

2. Sine-pulse width modulation: UNIPOLAR switching

This switching scheme treats each switch in Figure 4 as an individual vice a pair as in bipolar switching. An additional equal but opposite reference signal ($-v_{control}$) is also utilized as shown in Figure 6.

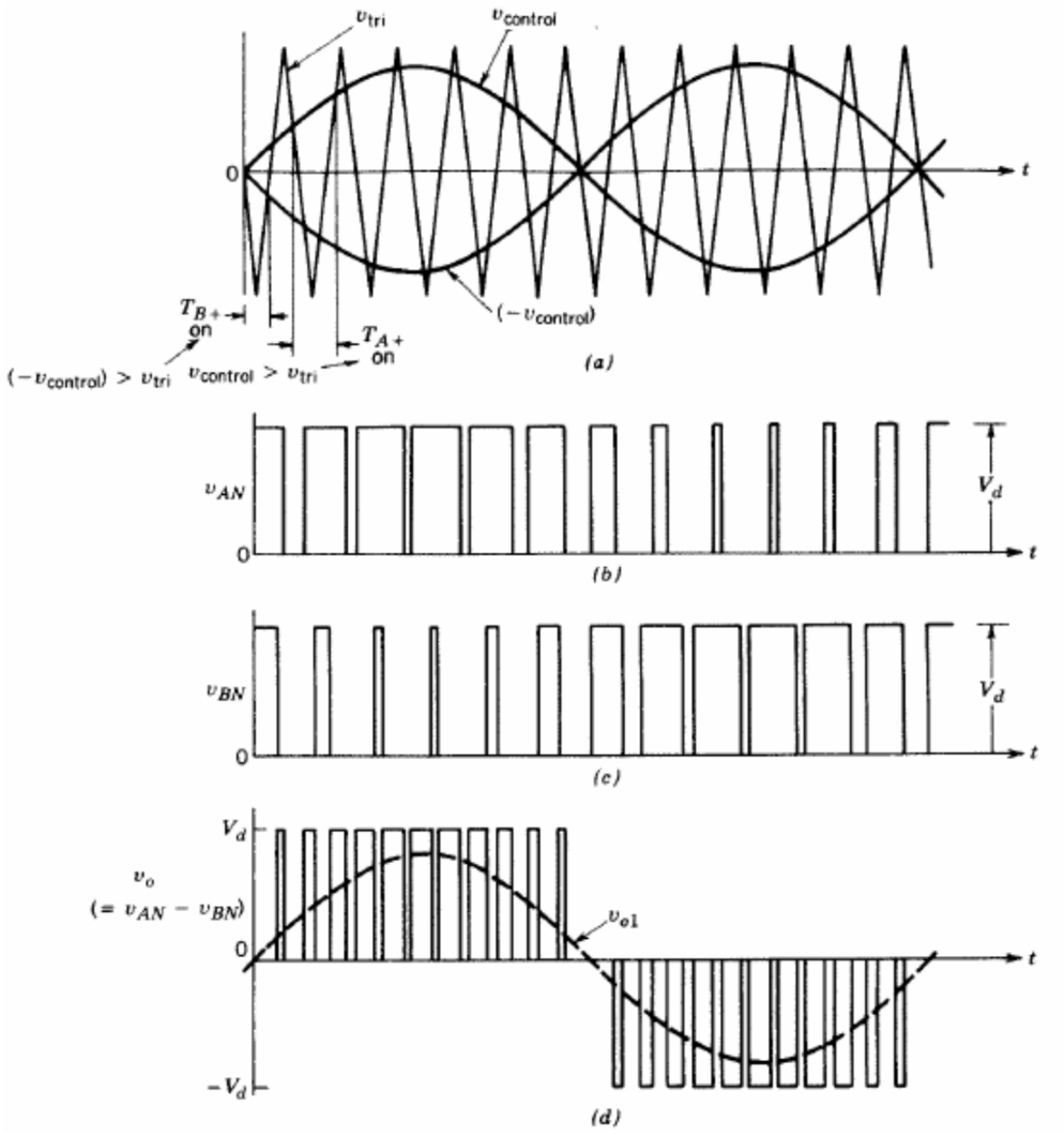

Figure 6. PWM with unipolar voltage switching (single phase). From [6].

The switches operate as follows [6]:

$$v_{control} > v_{tri}, \quad T_{A+} \text{ is on}, \quad v_{AN} = V_d \tag{3}$$

$$v_{tri} > v_{control}, \quad T_{A-} \text{ is on}, \quad v_{AN} = 0 \tag{4}$$

$$(-v_{control}) > v_{tri}, \quad T_{B+} \text{ is on}, \quad v_{BN} = V_d \tag{5}$$

$$(-v_{control}) < v_{tri}\ , \quad T_{B-} \text{ is on}, \quad v_{BN} = 0 \tag{6}$$

The output voltage v_o is equal to $v_{AN} - v_{BN}$ resulting in the output waveform shown in Figure 6.

One key advantage of this switching scheme is that it has the effect of doubling the switching frequency. This can be seen in Figure 7, a 15 kHz switching frequency applied to an H-bridge inverter utilizing bipolar PWM has a prominent peak at 15 kHz. The same switching frequency utilizing unipolar PWM results in a dominant peak at 30 kHz with a lower magnitude and lower total harmonic distortion (THD). Therefore, unipolar switching is the method used for the construction and simulation of the EMS built for this thesis.

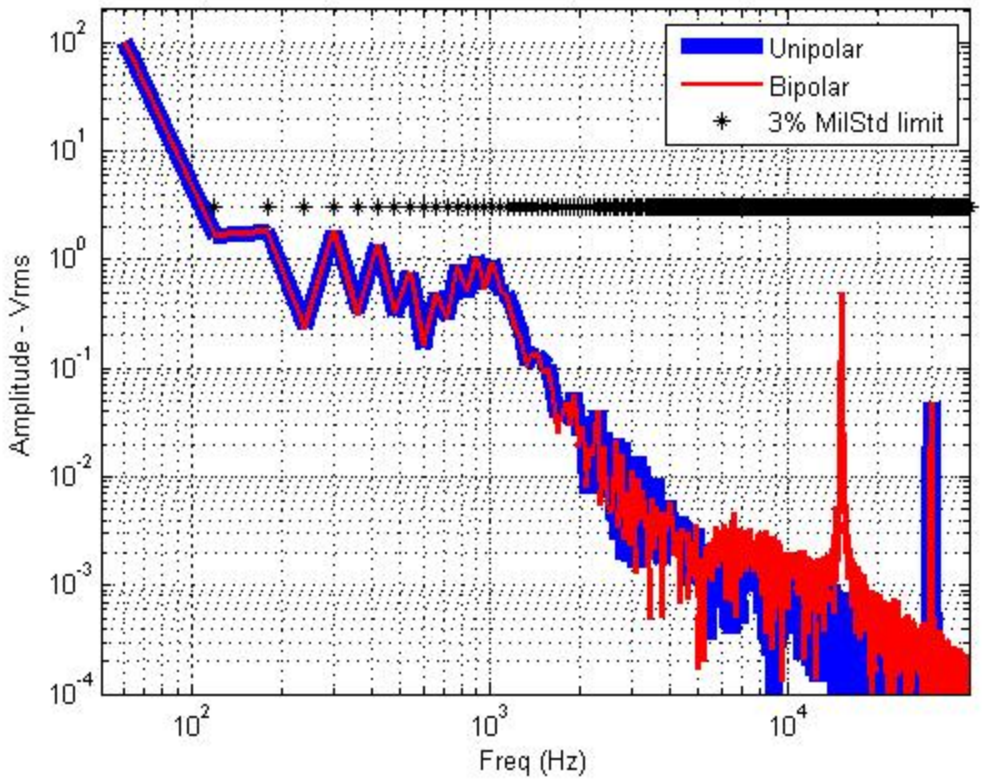

Figure 7. Unipolar vs bipolar harmonic simulation analysis.

D. EMS HARDWARE

The system constructed in the laboratory (as seen in Figure 9) is comprised of three printed circuit boards (PCB). Two of the three boards were built and tested in the

lab to support thesis research. A simplified functional block diagram of the EMS is shown in Figure 8. At the heart of the system is an FPGA which allows rapid changes to the system to aid in laboratory experimentation and validation. A universal serial bus (USB) interface is used to communicate from the PC to the FPGA through a Joint Test Action Group (JTAG or IEEE Standard 1149.1) programming cable. The top board (constructed in the lab) is comprised of the USB connector and interface chip used to communicate to the PC. The middle board (not constructed in the lab) is the FPGA development board. The bottom board contains the IGBT power module used for the power switches of the H-bridge and the boost converter, DC power supply, current/voltage sensors, and passive filtering components.

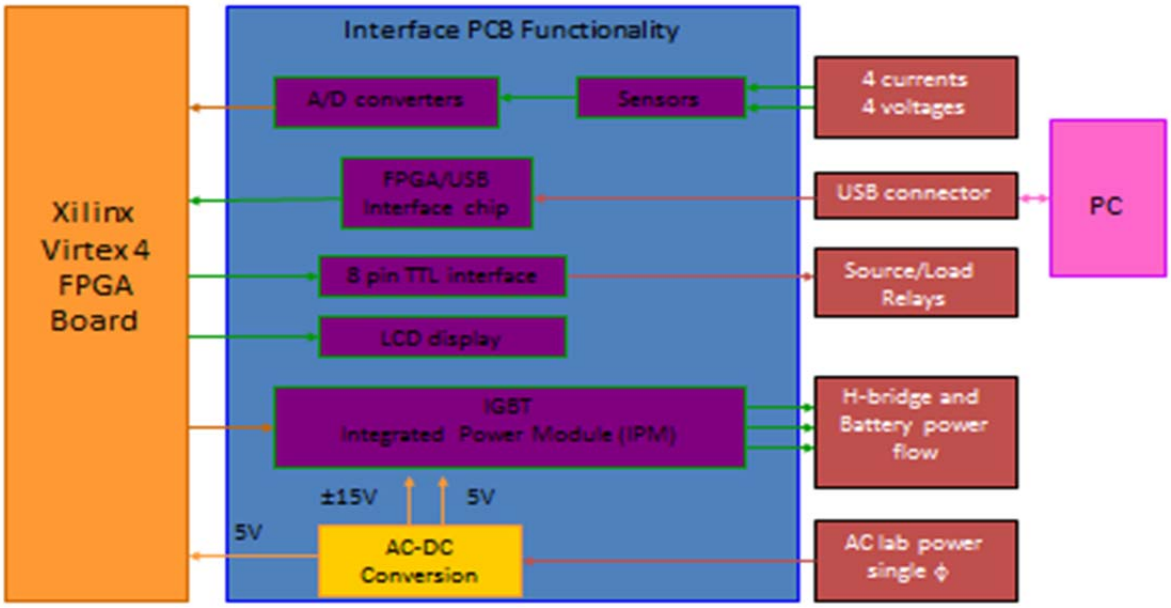

Figure 8. Block diagram of EMS.

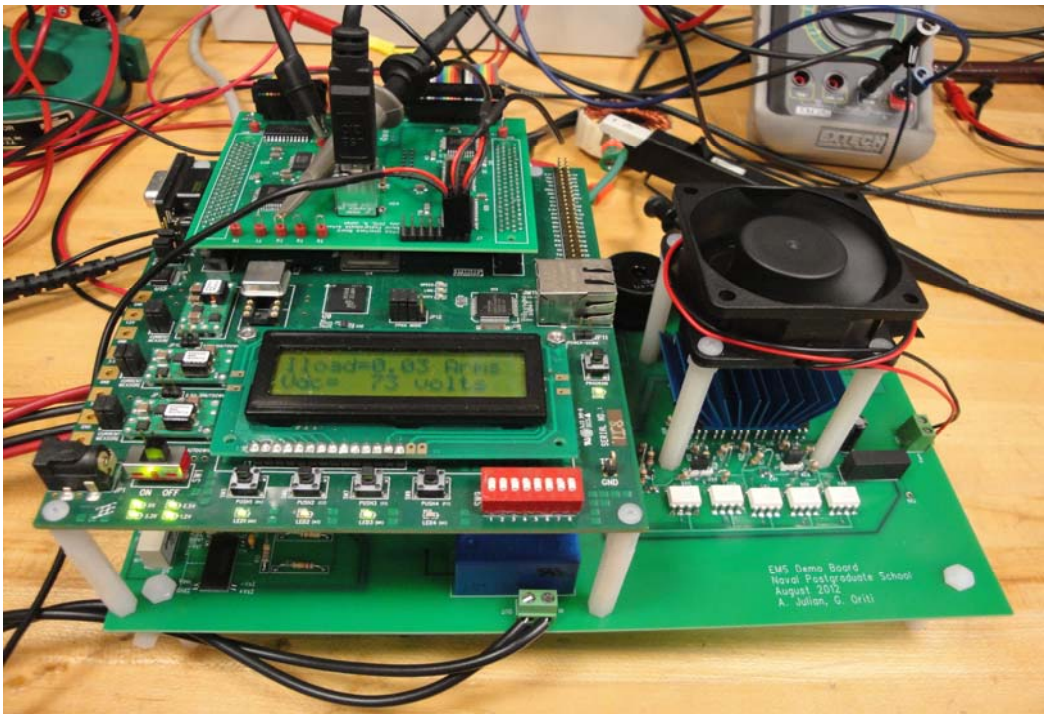

Figure 9. Image of laboratory built EMS.

THIS PAGE INTENTIONALLY LEFT BLANK

IV. H-BRIDGE LOADING MODEL AND SIMULATION

A. INTRODUCTION

The modeling of two scenarios of the lab built open loop H-bridge inverter connected to a diode rectifier or linear load through a passive filter as shown in Figure 10 and Figure 11, respectively, is detailed in this chapter. First to be covered is the modeling of the PWM signals to the switches. Next is the passive filter, and lastly, is the linear and diode rectifier load. The top-level Simulink block diagram of Figure 10 and Figure 11 is shown in Figure 12.

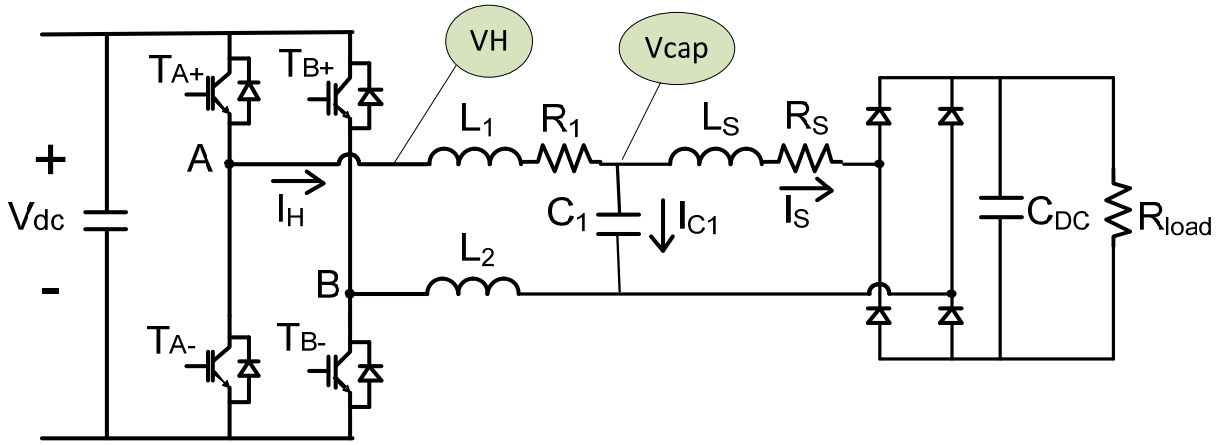

Figure 10. Simplified schematic of lab built H-bridge inverter with diode rectifier.

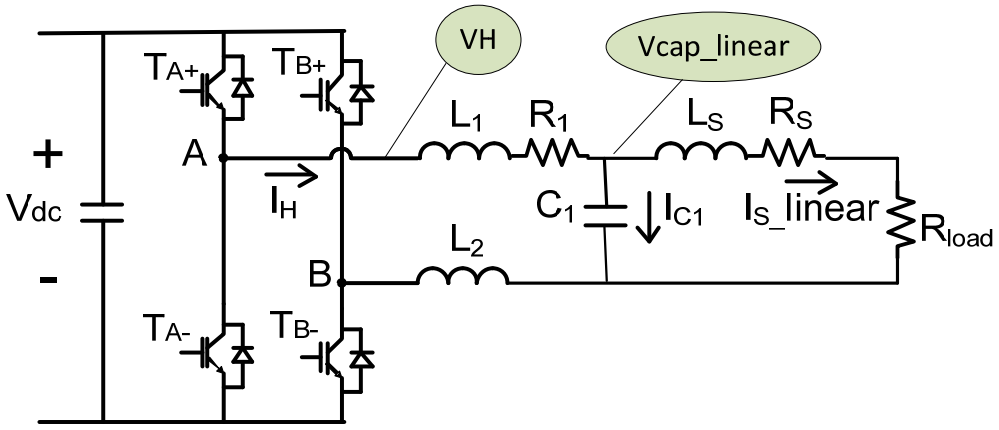

Figure 11. Simplified schematic of lab built H-bridge inverter with linear load.

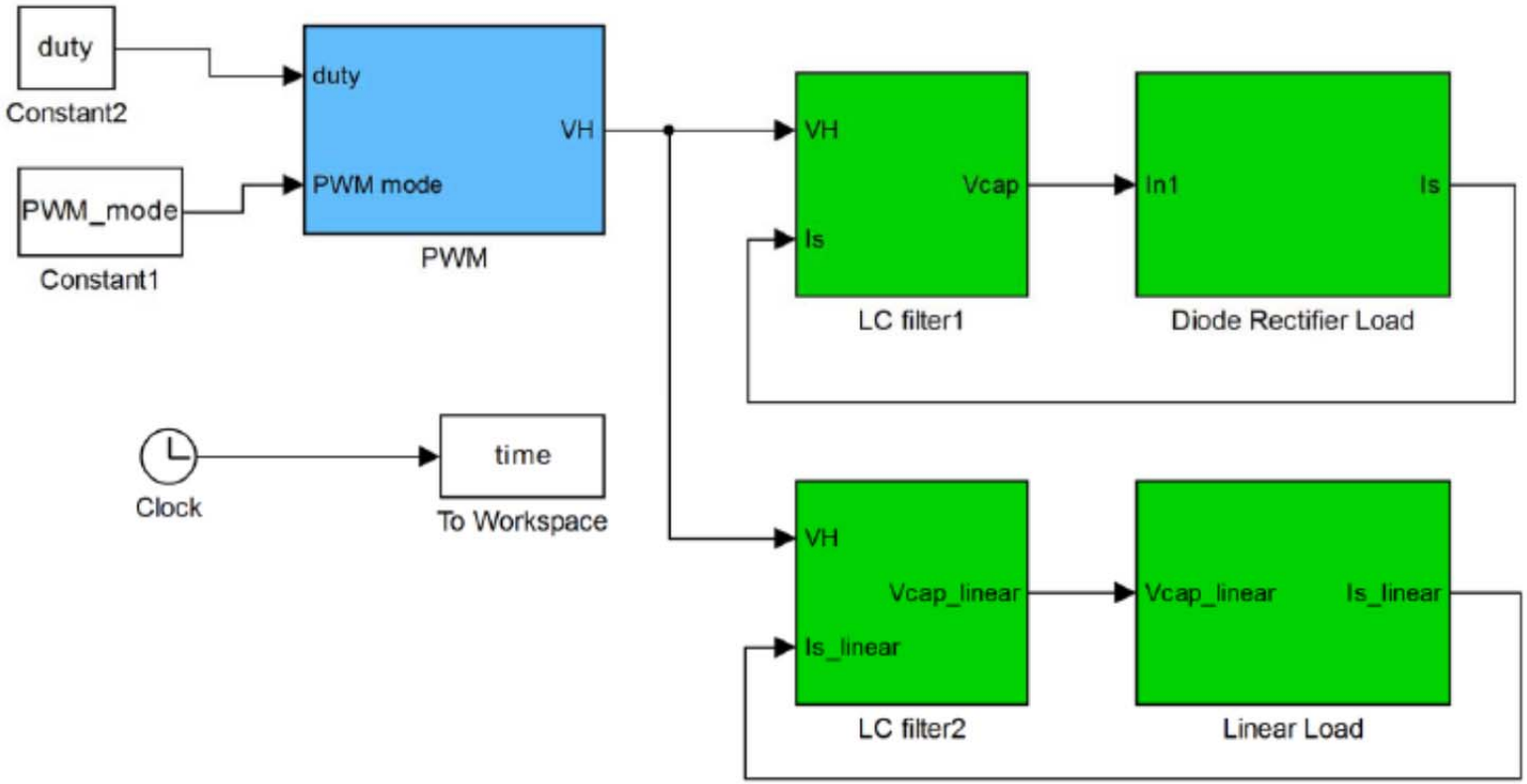

Figure 12. Top-level Simulink model of lab built H-bridge inverter w/loads.

B. PWM

In order to generate the gate signals to the H-bridge switches, the triangle waveform (v_{tri}) and control waveform ($v_{control}$) discussed in Chapter III (inverter theory) had to be formed. To generate v_{tri}, the arcsine of a 15 kHz (switching frequency) sine wave was taken as shown in Figure 13. The control wave, $v_{control}$, is a 60 Hz sine wave. Input 1 is used to manually adjust the duty cycle. Input 2 is used to switch between unipolar and bipolar PWM. Unipolar switching is used exclusively for this thesis. The output voltage of the H-bridge inverter is *VH*, and V_{DC} is the output of the boost converter on the PCB and also the DC bus voltage of the H-bridge inverter.

C. LC FILTER

A physics-based model of the LC filter shown in Figure 10 composed of L_1, L_2, R_1, and C_1 is depicted in Figure 14, where the LC filter1 and LC filter2 depicted in Figure 12 are identical with the exception of the input and output nomenclature. The voltage, V_{CAP}, is the capacitor C_1 voltage, while *IH* is the current drawn from the H-bridge inverter, I_S is the current drawn from the diode rectifier, and R_1 is in the model to account for inductor resistance and other non-ideal resistances.

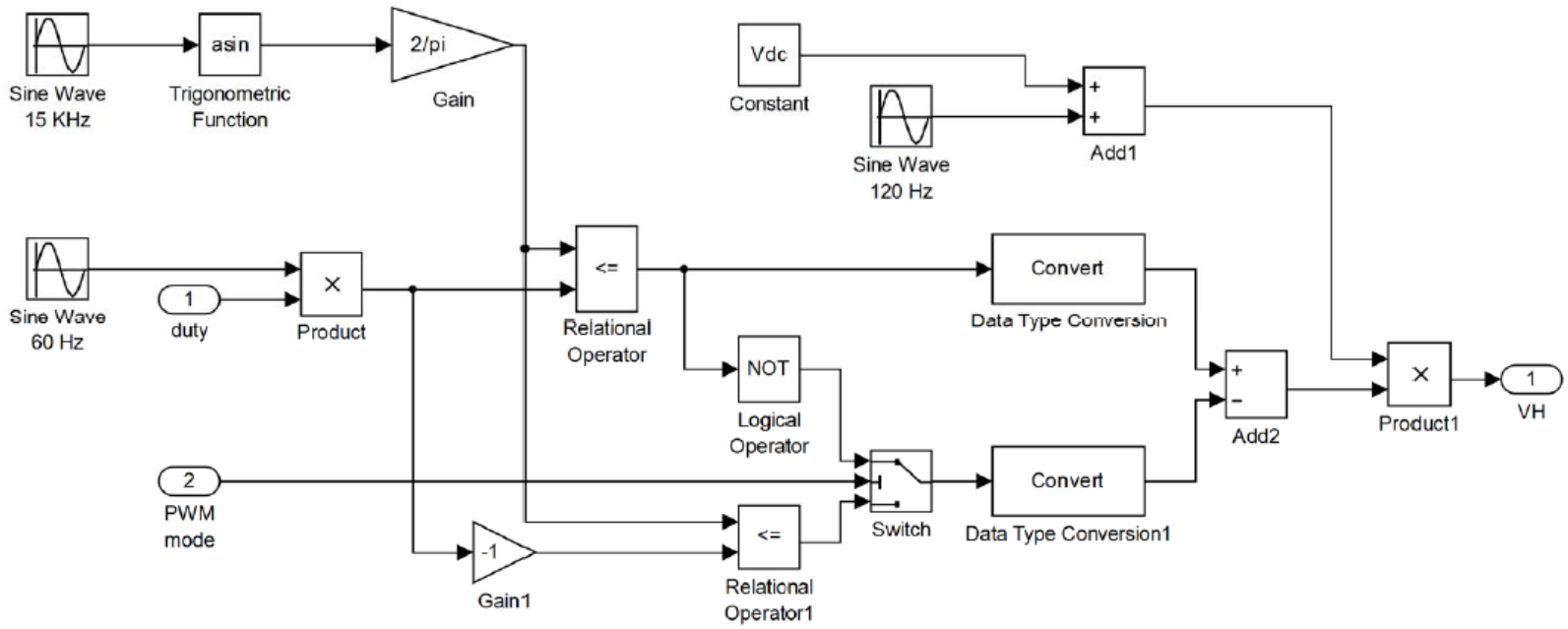

Figure 13. Simulink model of H-bridge inverter output voltage.

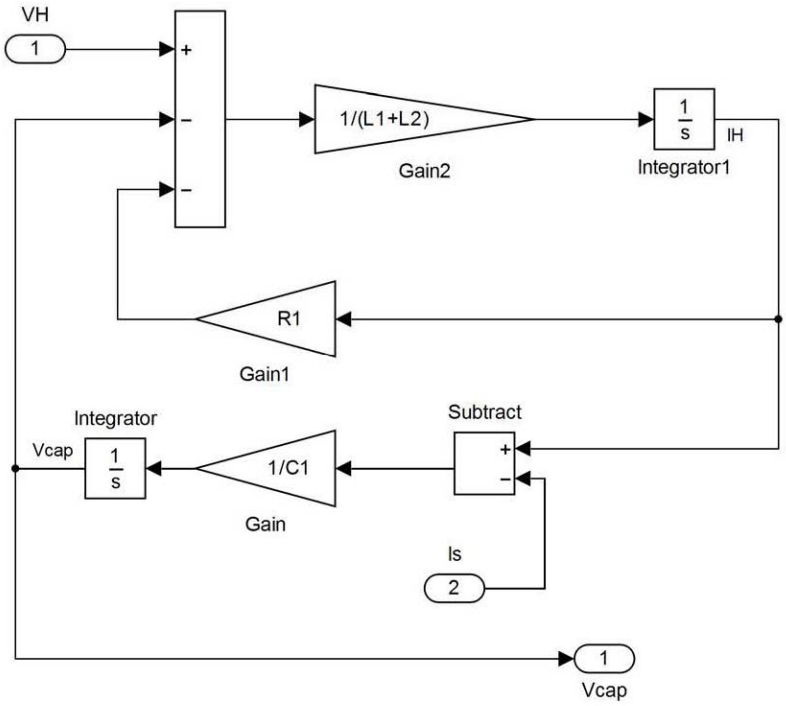

Figure 14. Simulink model of LC filter.

By examining Figure 10, we developed the physics based model shown in Figure 14 where *s* is the Laplace operator which leads to

$$V_{AB} - I_H s\left(L_1 + L_2\right) - I_H R_1 - I_{C1}\left(\frac{1}{sC_1}\right) = 0, \tag{7}$$

$$I_H = I_{C1} + I_S, \tag{8}$$

$$I_H = \frac{V_{AB} - I_H R_1 - \dfrac{I_H}{sC_1} - \dfrac{I_S}{sC_1}}{s\left(L_1 + L_2\right)}, \tag{9}$$

and

$$V_{cap} = I_{C1}\left(\frac{1}{sC_1}\right) = \left(I_H - I_S\right)\left(\frac{1}{sC_1}\right). \tag{10}$$

D. LINEAR LOAD

The physics-based model for a simple resistive load R_{load} was connected directly to the output of the LC filter to compare to acquired laboratory data. The Simulink model for this load is shown in Figure 15.

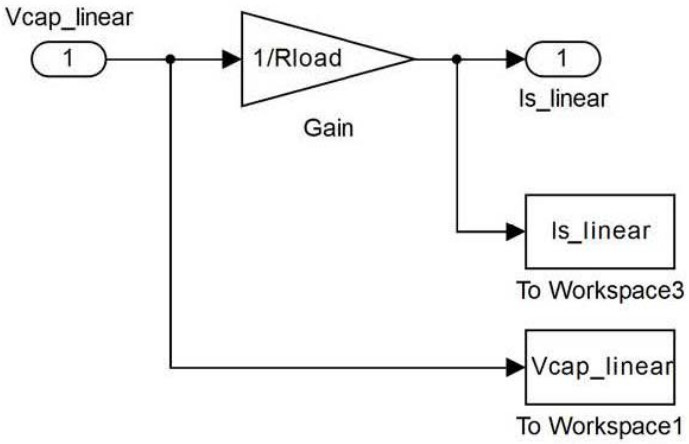

Figure 15. Simulink model of linear load.

E. DIODE RECTIFIER

The physics-based model of the diode rectifier circuit shown in Figure 16 is shown in Figure 17. The model develops a DC bus voltage across C_{DC}. The diode load current I_s is fed back to the LC filter1 block in Figure 12 to satisfy the physical equations for an accurate model. The components L_S and R_S are not actual components used for the EMS, but are used to develop a mathematical representation of the diode load current I_s. Also, they are used to account for non-ideal stray inductance and resistance within the actual circuit.

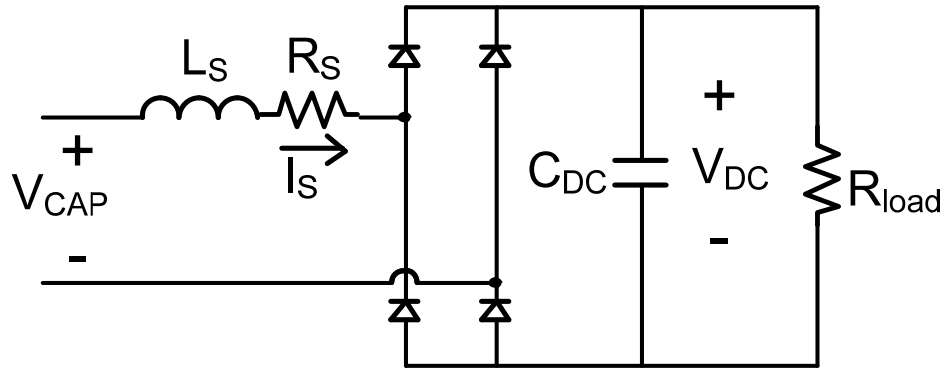

Figure 16. Modeled diode rectifier circuit.

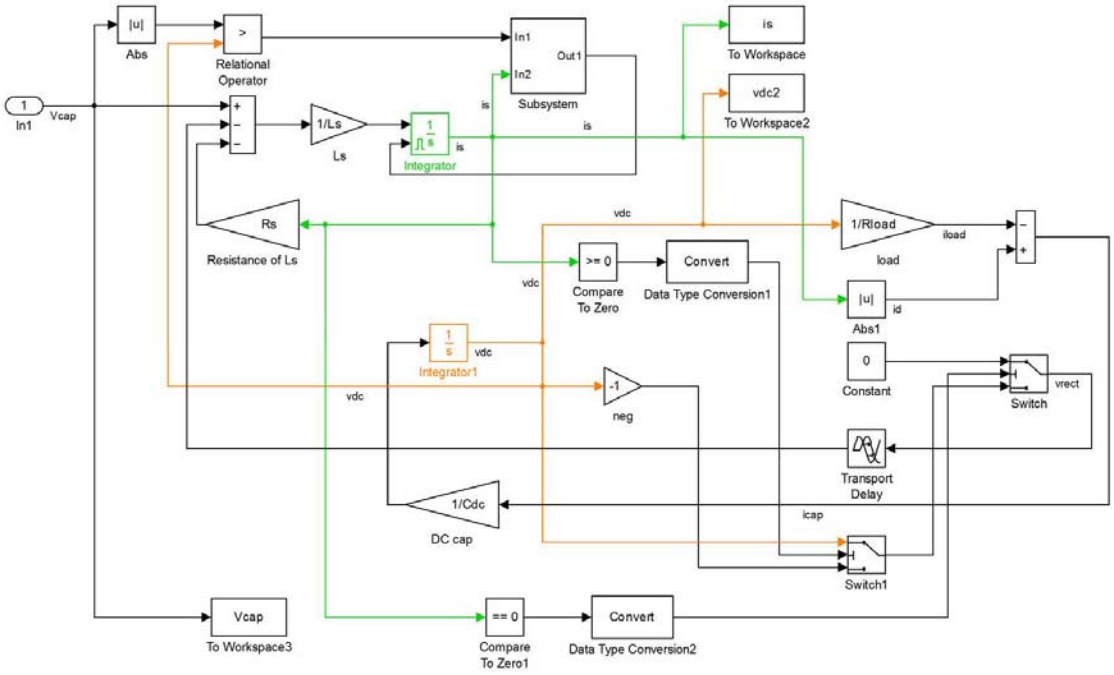

Figure 17. Diode rectifier Simulink model.

Active filtering was researched in evaluating the methods to reduce the voltage THD on the output of the H-bridge inverter. An active filter injects current to the load to achieve a more sinusoidal line voltage. However, [7] suggests that an active filter is not helpful for passive diode rectifiers. The simulated voltage (labeled V_{CAP} in Figure 10) and current (labeled I_s in Figure 10) are shown in Figure 18. To demonstrate the effects of an active filter, a 60 Hz sine wave of equal magnitude to the fundamental frequency without the active filter replaced input one of Figure 17. The result coincides with [7],

showing an increased diode peak current with a smaller conduction angle shown in Figure 19. This condition places additional stresses on the diode and is not preferred. In fact, the load needs to be modified to improve power quality. This can be accomplished with power factor correction rectifiers instead of passive diode rectifiers as discussed in [8]. This is the trend of future regulation and technology development.

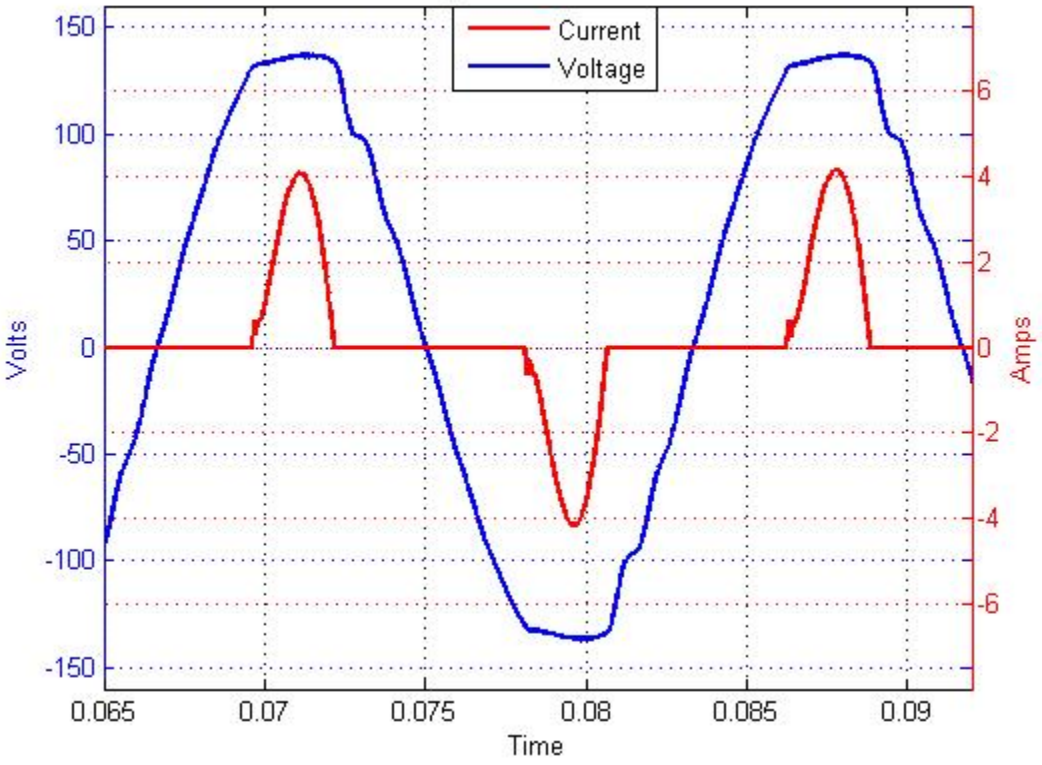

Figure 18. Modeled voltage and current.

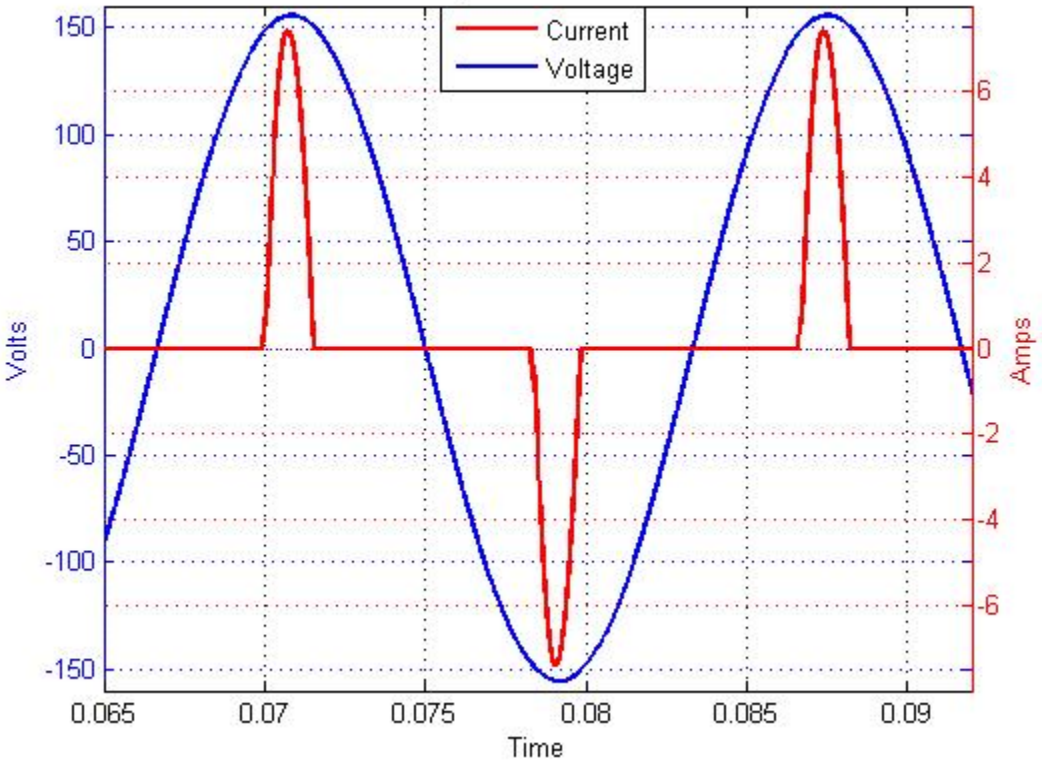

Figure 19. Modeled voltage and current with active filter

THIS PAGE INTENTIONALLY LEFT BLANK

V. SIMULATION AND LABORATORY TEST COMPARISON

A. INTRODUCTION

The EMS pictured in Figure 9 was built and tested in the laboratory. The physical construction is based on the schematics illustrated in Figure 10 and Figure 11. The parameter L_1 is comprised of 470 μH and 230 μH inductors placed in series, while C_1 is a 12 μF film capacitor and L_2 is a 470 μH inductor. The components R_1, R_S, and L_S of Figure 10 are model parameters to account for non-ideal components. The capacitor C_{DC} is a 2000 μF electrolytic capacitor. The load R_{LOAD} is comprised of three resistors (300 Ω, 600 Ω, and 1200 Ω) in parallel, and V_{DC} was set to 200 V by the use of a boost converter. The PWM frequency was set to 15.7 kHz. Lastly, the duty cycle was set to 0.78.

B. DIODE RECTIFIER LOAD

The filtered output V_{CAP} of the H-bridge inverter is shown in Figure 20. The THD of the simulated V_{CAP} was evaluated to be 3.7%, which is below the MIL-STD-1399-300B limit of 5%. The individual voltage harmonics are also below the MIL-STD-1399-300B limit of 3% as shown in Figure 21. THD is defined by

$$THD = \frac{\sqrt{\sum_{h=2}^{\infty} V_h^2}}{V_1}. \tag{11}$$

An image of the laboratory scope is shown in Figure 25. The labeled waveform *Vcfil* is the voltage across capacitor C_1 (labeled V_{CAP} in Figure 10), while *Iems* is the current supplied from the H-bridge inverter (labeled *IH* in Figure 10), and *Iload* is the current supplied to the diode rectifier (labeled I_S in Figure 10). The flat-topped waveform *Vcfil* is due to the charging of capacitor C_{DC}. When the load R_{LOAD} is reduced, the amount of flat-topping is also reduced.

Utilizing a Tektronix model MSO 4034 oscilloscope's data acquisition feature, we were able to import this data into MATLAB for display and harmonic analysis. The

imported voltage waveform across capacitor C_1 which closely resembles that of the simulation results is shown in Figure 20. The THD of V_{CAP} was evaluated to be 4.7%. There is also a large third order harmonic evaluated to be 3.48%, which can be seen in Figure 21. It is also noted that the harmonics of the simulation dropped more quickly with frequency, which was attributed to many non-ideal conditions such as voltage drop across diode, rise and fall time of the IGBT switching, and voltage drop across the IGBTs not being properly accounted for. However, the amplitude of all of the higher order harmonics are still very small in the laboratory results

The THD for both the model and laboratory test was only slightly below the 5% MIL-STD-1399-300B limit. Evaluation of the individual harmonics resulted in the third order harmonic from the laboratory exceeding the 3% individual harmonic limit of MIL-STD-1399-300B.

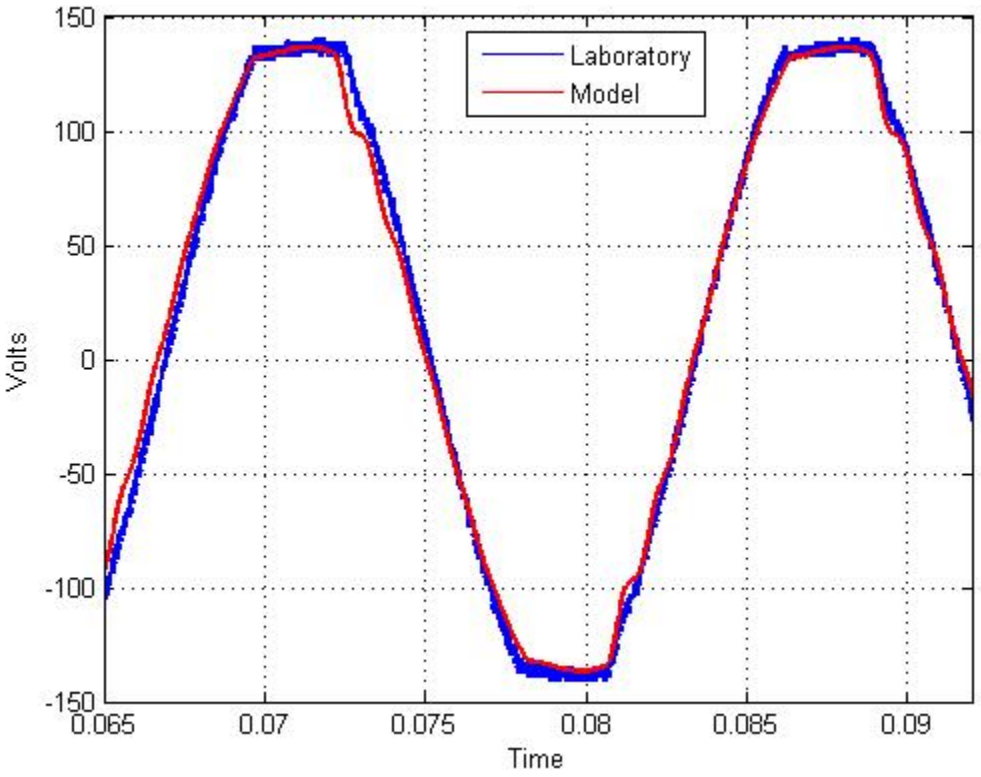

Figure 20. Simulated and measured H-bridge output filtered voltage with rectifier load.

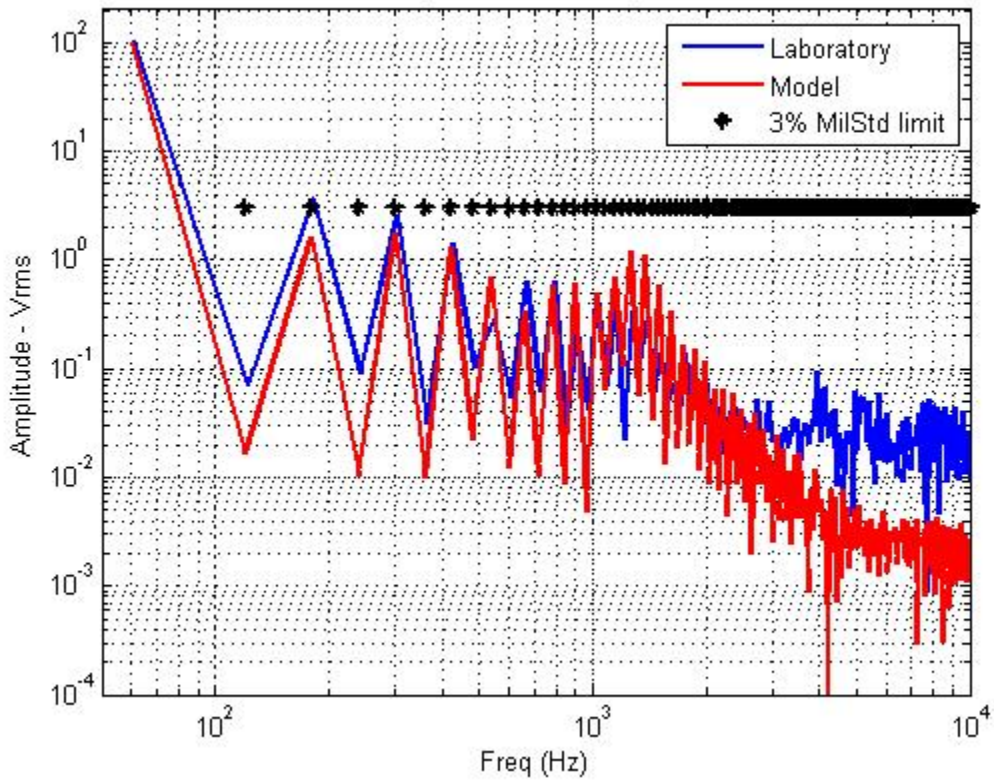

Figure 21. H-bridge output filtered voltage harmonics with rectifier load and 120 Hz ripple included on DC bus.

Distortion factors that are idealized in the simulation easily show up in the frequency analysis as shown in Figure 21. The idealized simulation model does not account for IGBT voltage drop, diode voltage drop, switching rise/fall time, and blanking time. The calculated resonance f_o of the circuit, 1.34 kHz, accounts for the rise in amplitude at that point. The resonance frequency is defined by

$$f_o = \frac{1}{2\pi\sqrt{LC}}. \tag{12}$$

When the 120 Hz ripple on the VSI DC bus is included in the simulation, the voltage harmonics are affected. This ripple is a consequence of the DC bus regulator trying to compensate for the pulsating power drawing by the single phase load. The effect of excluding the 120 Hz ripple from the DC bus can be seen by comparing Figure 21 which includes the 120 Hz ripple, with Figure 22.

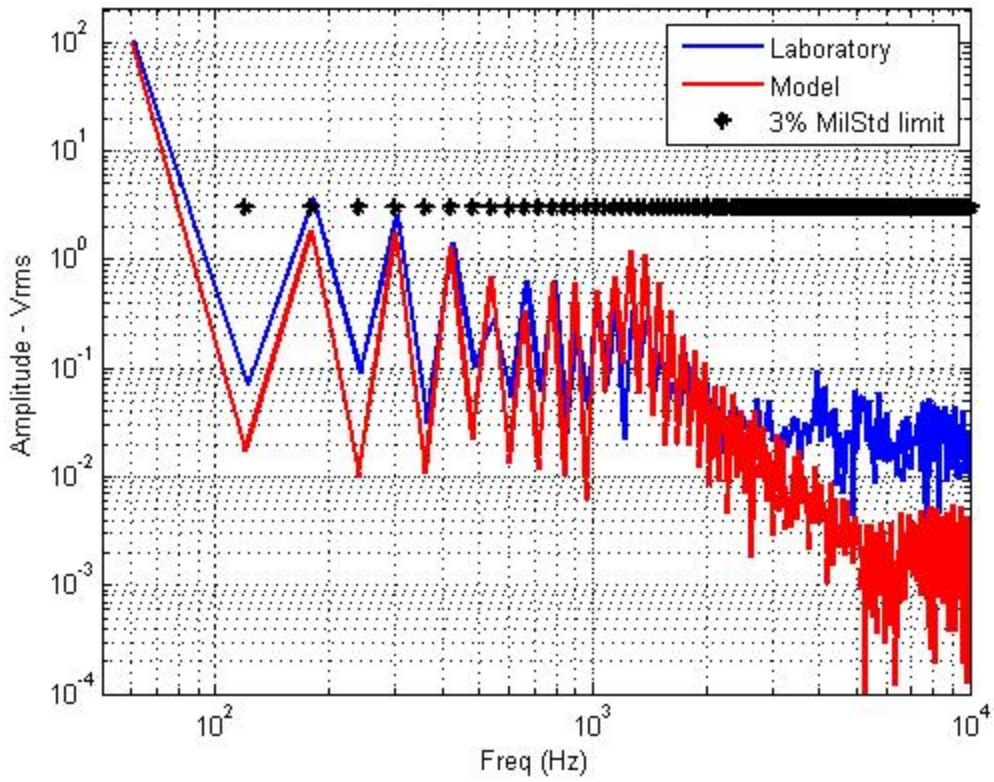

Figure 22. H-bridge output filtered voltage harmonics with rectifier load and 120 Hz ripple excluded on DC bus.

The load current *Is* is shown in Figure 23. The current pulses correspond to the flat-topped voltage waveform of Figure 20 as the rectifier draws current when the voltage of capacitor C_{DC} is less than the voltage across capacitor C_1. Like the voltage waveform comparison, the simulation and laboratory currents are very similar.

The operation of user equipment with power ratings less than 1 kVA must be current amplitude limited so that no individual harmonic line current or current of any frequency above the fundamental at 60 Hz to 20 kHz exceeds the limit line set at a magnitude of 6000/*f* percent of the user equipment's full load fundamental current, where *f* is the frequency [9]. The results of the laboratory and model with a load of 171 Ω are shown in Figure 24. The simulated load was reduced to 70 Ω, at which point the model showed a third voltage harmonic above the 3% limit. Analysis of the individual line currents proved to remain out of specification for this design.

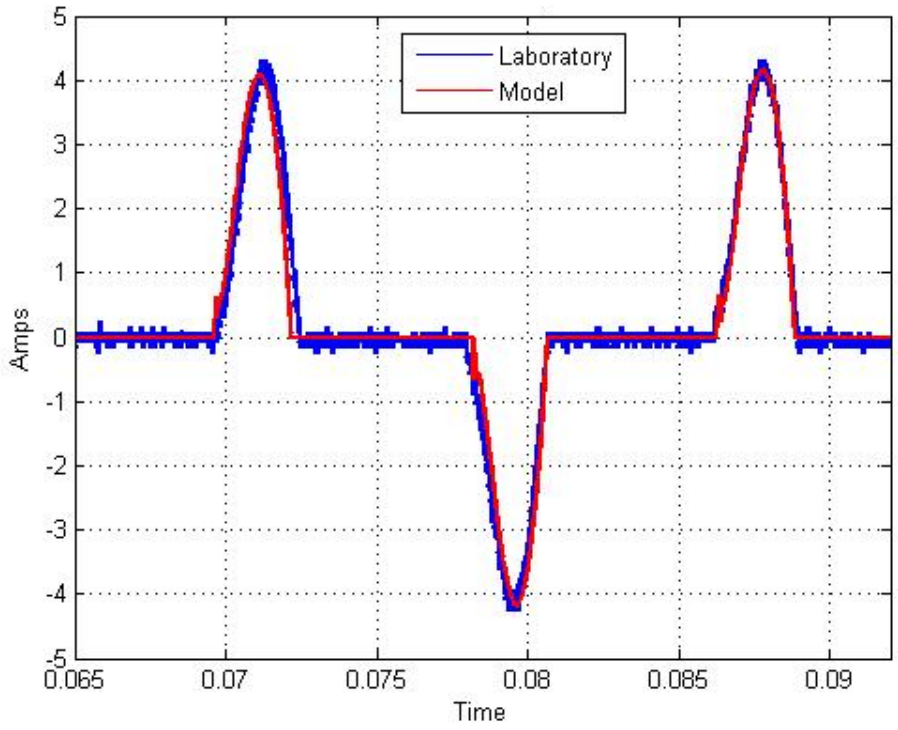

Figure 23. Simulated and measured H-bridge output rectifier load current.

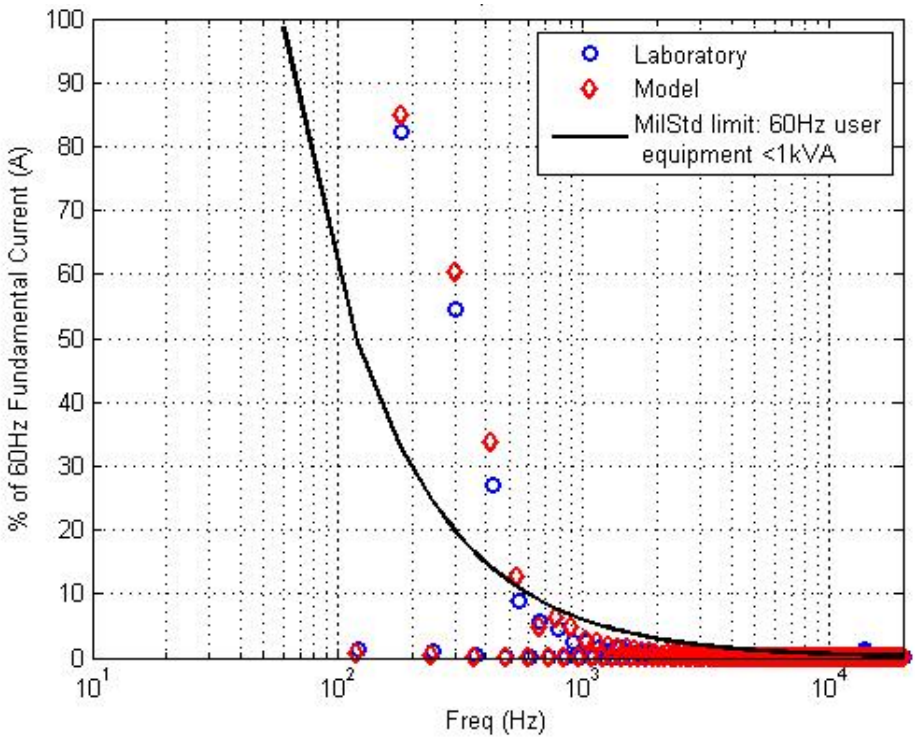

Figure 24. Individual harmonic line currents with rectifier load.

Figure 25. Oscilloscope image with diode rectifier load and EMS disconnected from the grid (channel 1 AC voltage, channel 2 EMS output current, channel 3 load current, channel 4 source current).

C. LINEAR LOAD

The simulated filtered output V_{CAP_LINEAR} of the H-bridge inverter with linear load is shown in Figure 26. The THD of V_{CAP} was evaluated to be 0.4%, which is well below the MIL-STD-1399-300B limit of 5%. The individual harmonics are also below the MIL-STD-1399-300B limit of 3% as shown in Figure 27. Like the analysis done for the diode rectifier load, the resonance of the circuit is unchanged. The circuit resonance of 1.34 kHz shows up in the harmonic analysis around that frequency.

When the 120 Hz ripple on the VSI DC bus is included in the simulation, the voltage harmonics are affected. This ripple is a consequence of the DC bus regulator trying to compensate for the pulsating power drawing by the single-phase load. The effect of excluding the 120 Hz ripple on the DC bus can be seen by comparing Figure 27, which includes the 120 Hz ripple to Figure 28.

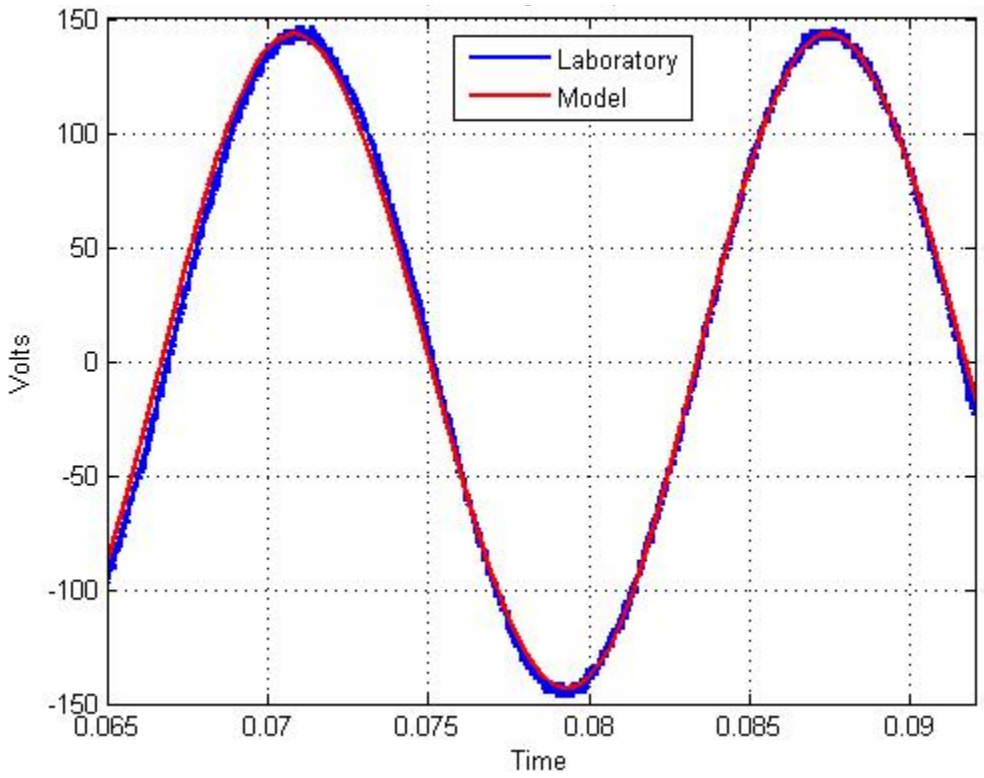

Figure 26. Simulated and measured H-bridge output filtered voltage with linear load.

Like the output voltage shown in Figure 26, the load current drawn by *Rload* closely matches that of the developed physics-based model as shown in Figure 29.

The operation of user equipment with power ratings less than 1 kVA must be current amplitude limited so that no individual harmonic line current or current of any frequency above the fundamental at 60 Hz to 20 kHz exceeds the limit line set at a magnitude of 6000/*f* percent of the user equipment's full load fundamental current, where *f* is the frequency [9]. The results of the laboratory and model with a load of 171 Ω are shown in Figure 30. All individual harmonic line currents remained less than 10%. However, the laboratory results showed an out-of-specification condition near the 15 kHz switching frequency. This was determined to be from the non-ideal source, as one would not expect to have current line harmonics from an ideal source. MIL-STD-1399-300B has much tighter specifications on loads than it does power sources, as the output voltage from the VSI is within specification. Figure 31 is a screen capture of the oscilloscope display during lab testing.

Figure 31 is a screen capture of the oscilloscope display during lab testing. The labeled waveform *Vcfil* is the voltage across capacitor C_1 (labeled V_{CAP_LINEAR} in Figure 11), while *Iems* is the current supplied from the H-bridge inverter (labeled I_H in Figure 11), and *Iload* is the current supplied to the linear load (labeled I_S*_linear* in Figure 11). Again, utilizing the scope's data acquisition feature, we were able to import this data into MATLAB for display and harmonic analysis. The imported voltage waveform across capacitor *C1* which closely resembles that of the simulation results, is shown in Figure 26. The THD of V_{CAP} was evaluated to be 0.8%. The individual harmonics obtained in the lab shown in Figure 26 are all below the 3% MIL-STD-1399-300B limit.

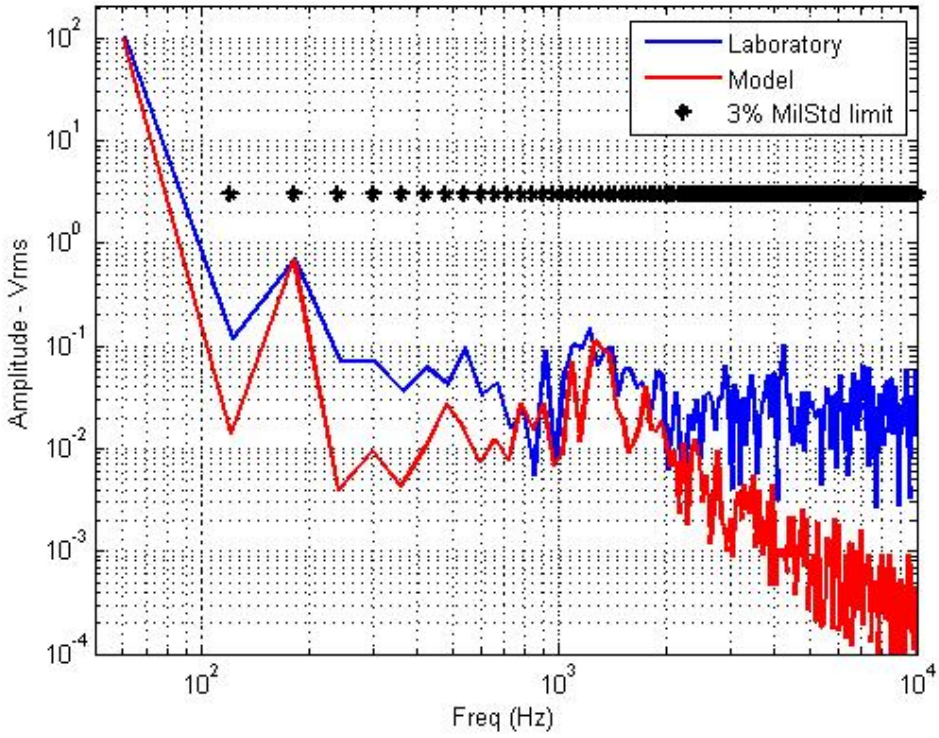

Figure 27. H-bridge output filtered voltage harmonics with linear load and 120 Hz ripple included on DC bus.

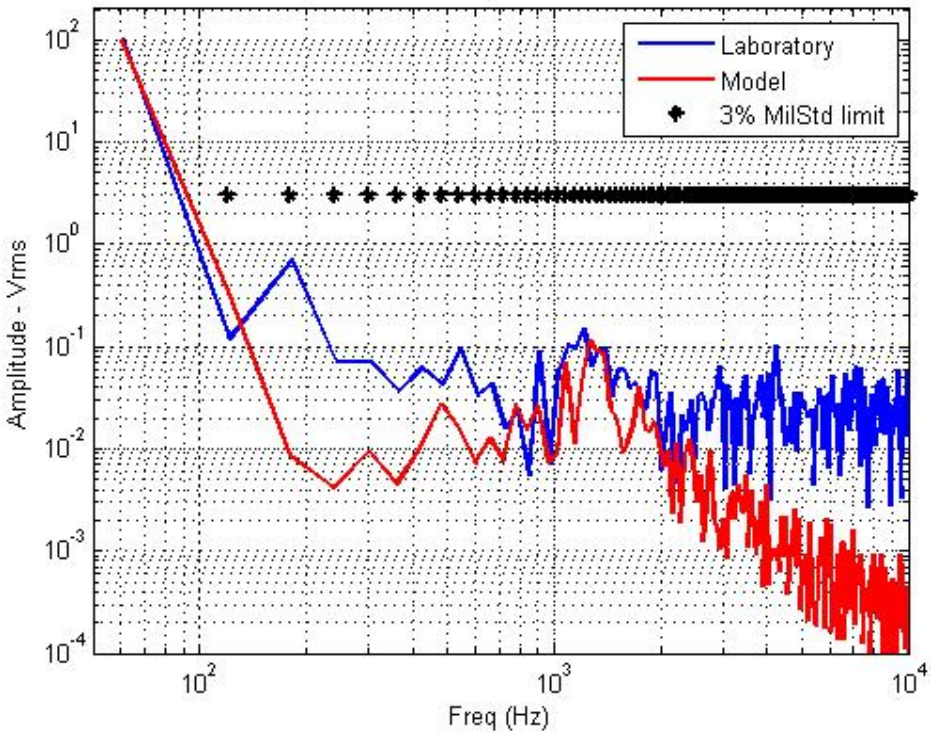

Figure 28. H-bridge output filtered voltage harmonics with linear load and 120 Hz ripple excluded on DC bus.

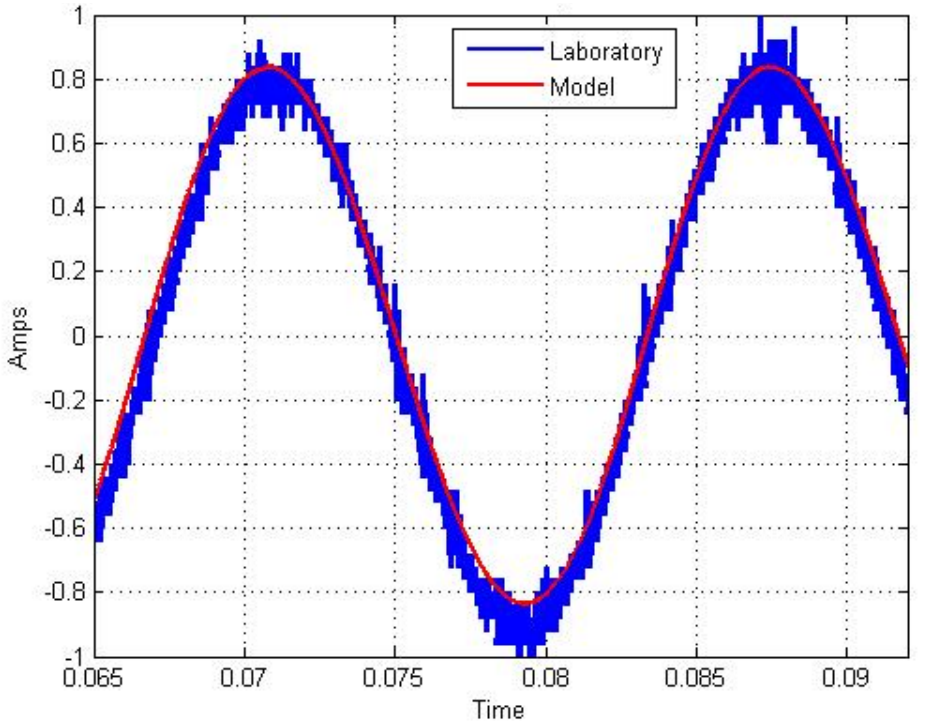

Figure 29. Simulated and measured H-bridge output linear load current.

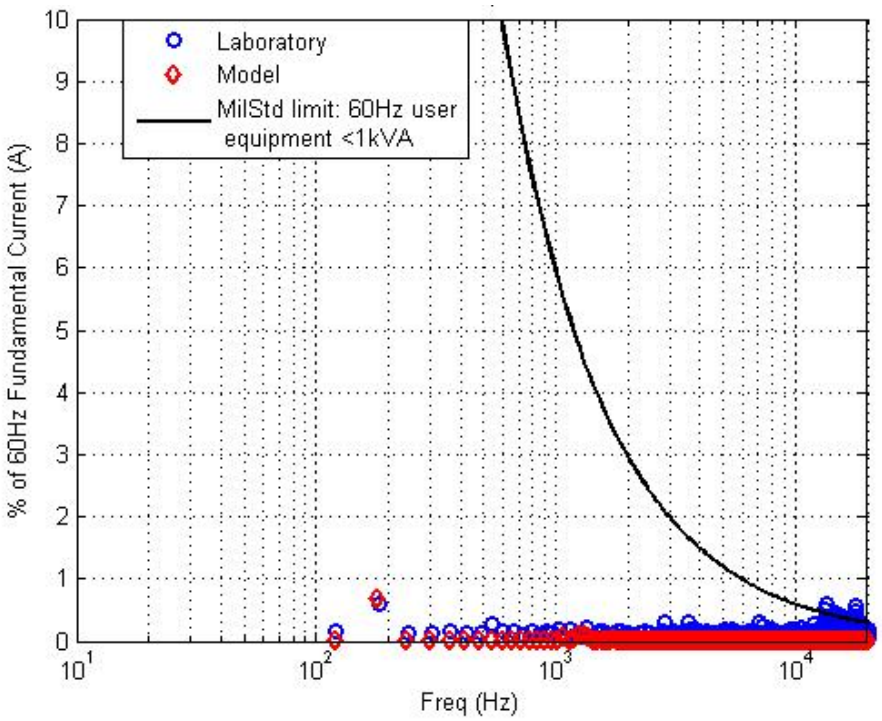

Figure 30. Individual harmonic line currents with linear load.

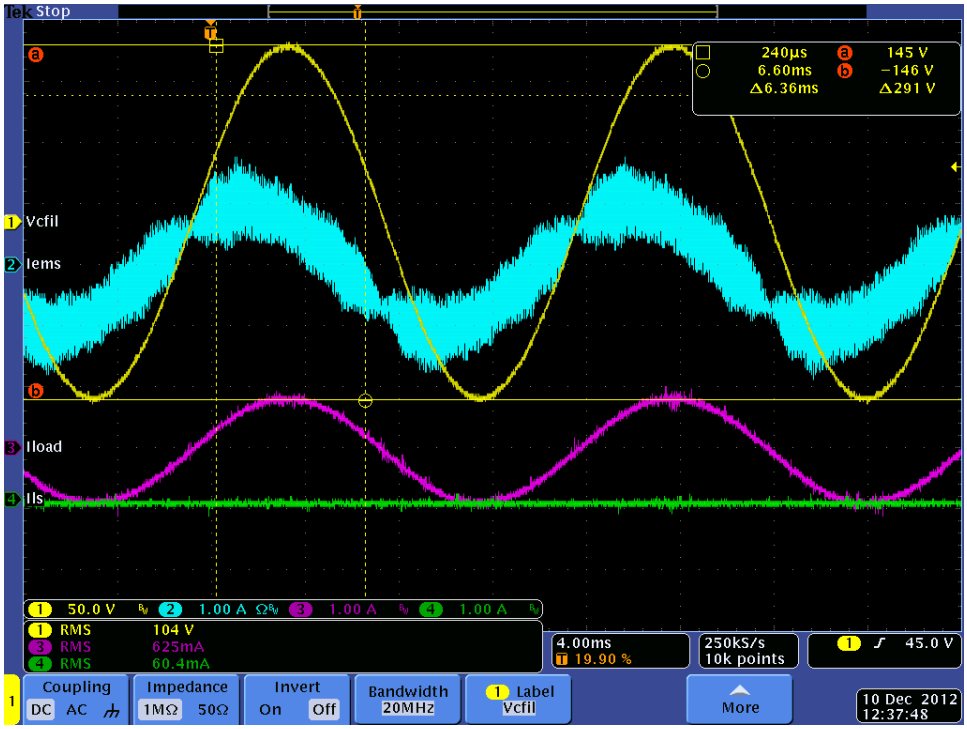

Figure 31. Oscilloscope Image with linear load and EMS disconnected from the grid (channel 1 AC voltage, channel 2 EMS output current, channel 3 load current, channel 4 source current).

VI. SIMULATION OF DIFFERENT LINEAR LOADS

A. INTRODUCTION

Through simulation and lab verification discussed in chapters IV and V, it was shown that a passive diode rectifier load supplied by a H-bridge inverter does not meet MIL-STD-1399-300B. However, the linear load simulated and lab verified as discussed in Chapter V was within specification. In this chapter, the effect of higher linear loading conditions is presented along with a simple control strategy to account for the voltage sagging encountered.

B. LINEAR LOADING EFFECTS

The linear load portion of the model shown in Figure 12 was modified and is pictured in Figure 32. By measuring the RMS input voltage to the linear load, a PI controller is able to adjust the duty cycle to maintain a constant output voltage level. The PI controller was connected to the EMS by modifying the circuit in Figure 11 to that shown in Figure 33.

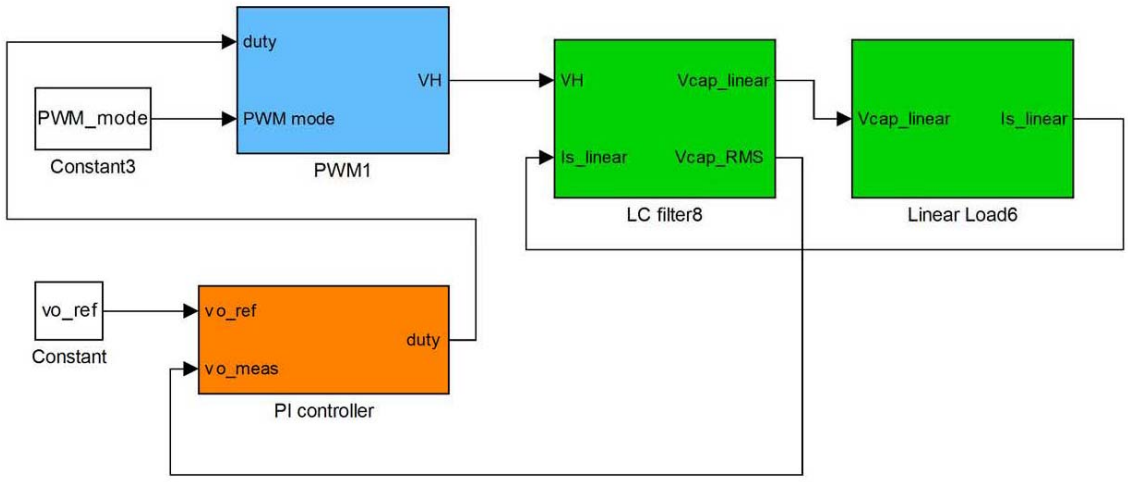

Figure 32. H-bridge model with linear load and controller.

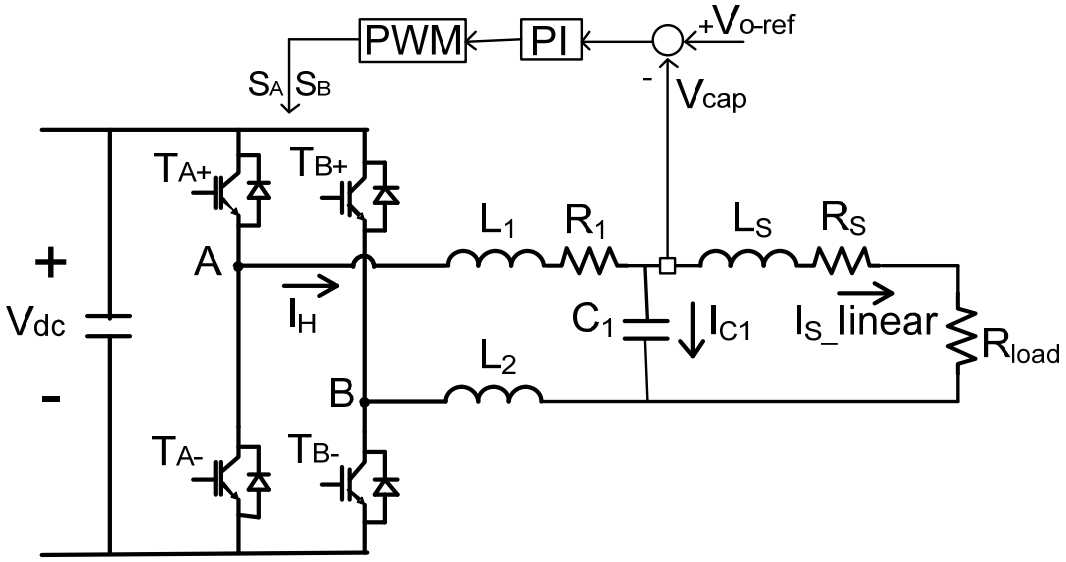

Figure 33. Connection of a PI controller to the EMS.

To demonstrate the need of a controller, the output voltage was simulated by increasing the linear load. The effects of the increased load with constant duty cycle are shown Figure 34. The peak output voltage sags as the load increases, and therefore, the RMS voltage sags. The RMS voltage is one of the simplest electrical power measurements to take. Therefore, a simple PI controller that measures the RMS output voltage and compares it to a reference was modeled as shown in Figure 32.

The PI controller regulates the output voltage by adjusting the duty cycle in order to maintain the output voltage constant. The simulated output voltage for a 25 Ω linear load with fixed and controlled duty cycle is shown in Figure 35. The controller increases the duty cycle to adjust for the increased load in order to maintain the reference value programmed. A load of 5 Ω or more resulted in a 100% duty cycle, at which time any further load increase has unavoidable voltage sag. A higher DC input bus voltage to the H-bridge is required for any increased loading once the duty cycle reached 100%.

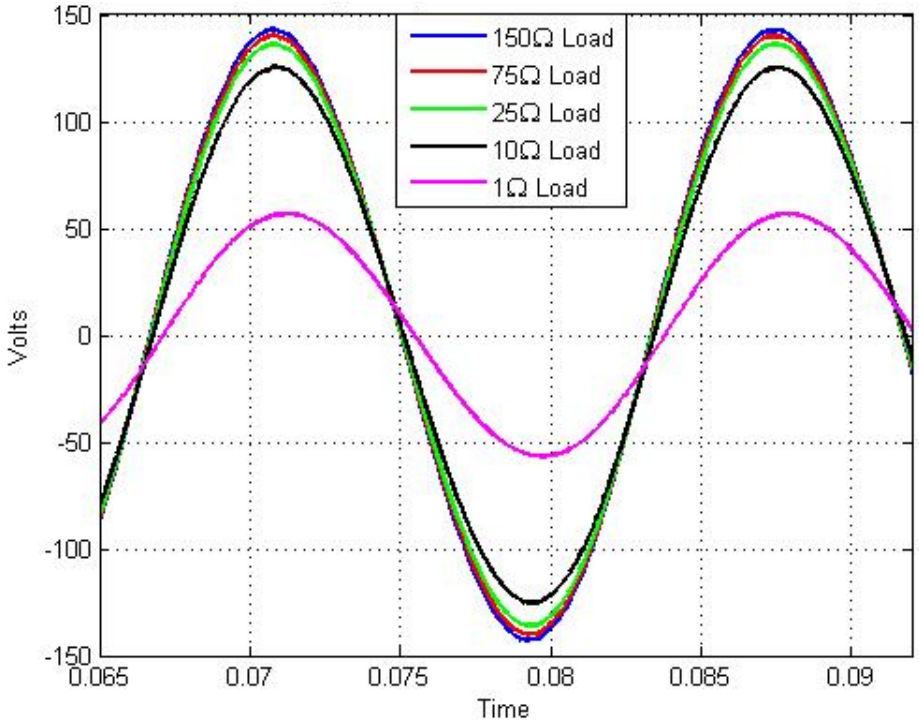

Figure 34. Simulated output voltage comparison with linear loads and constant duty cycle.

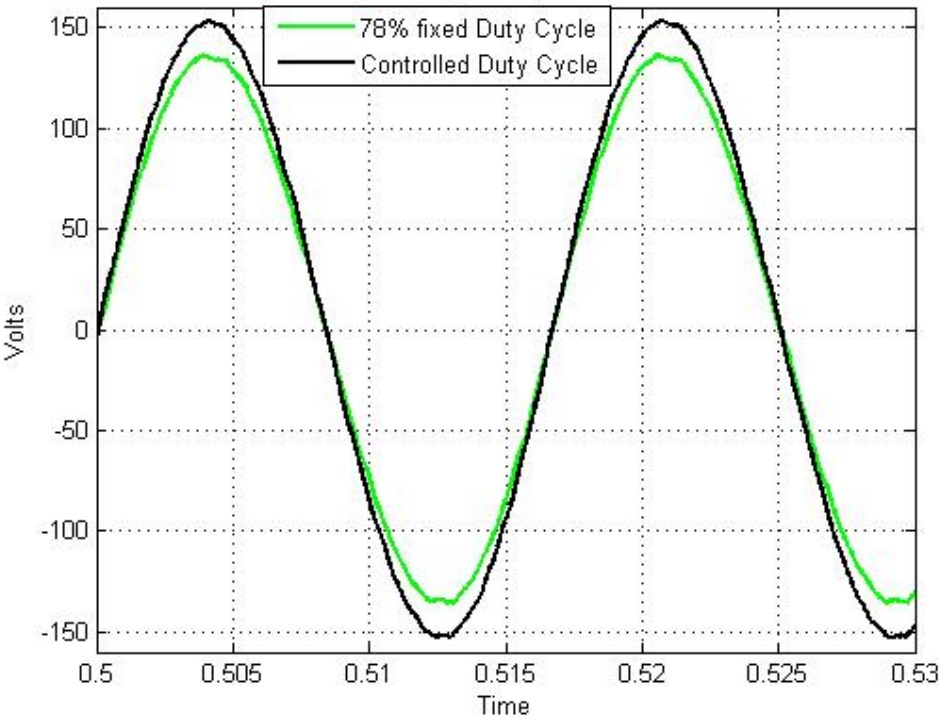

Figure 35. Simulated output voltage comparison with and without controller.

THIS PAGE INTENTIONALLY LEFT BLANK

VII. CONCLUSION

A. ACCOMPLISHMENTS

An evaluation of an open loop PWM single-phase H-bridge inverter was evaluated against MIL-STD-1399-300B in this thesis. The single-phase inverter is the main entity that makes up the EMS and can be configured to operate in many different scenarios through the use of a FPGA and software programming as discussed in Chapter II. In addition to the laboratory built EMS, a Simulink model of the H-bridge inverter with either a diode rectifier or linear load was evaluated against the physical EMS results.

The results of the model accurately predicted that of the hardware design. This is a crucial step in moving to high level model driven design that saves time and money. Through simulation and lab verification, the best PWM switching scheme, unipolar, was identified. It was also realized that a constant linear load can easily be operated open-loop while meeting MIL-STD-1399-300B, while dynamic linear loading would require a simple closed loop control (illustrated in Figure 32) in order to maintain the RMS output voltage due to voltage sagging at higher loads. No "wave-shaping" methods are required.

Out-of-specification line current harmonics with the EMS supplying a linear load were determined to be coming from the power source (VSI) itself. Even though the source was within specification per MIL-STD-1399-300B, it was unable to supply an ideal load.

Evaluation of the diode rectifier load connected to an H-bridge inverter did not meet MIL-STD-1399-300B specifications. Additional filtering would be required to reduce the harmonics. An increased load also results in a more flat-topped voltage waveform and higher THD to include individual harmonics. The research done in [7] and simulated in our model proves that active filtering is a non-ideal method to correct for this distortion with a passive diode rectifier load due to excessive diode current as seen in Figure 36.

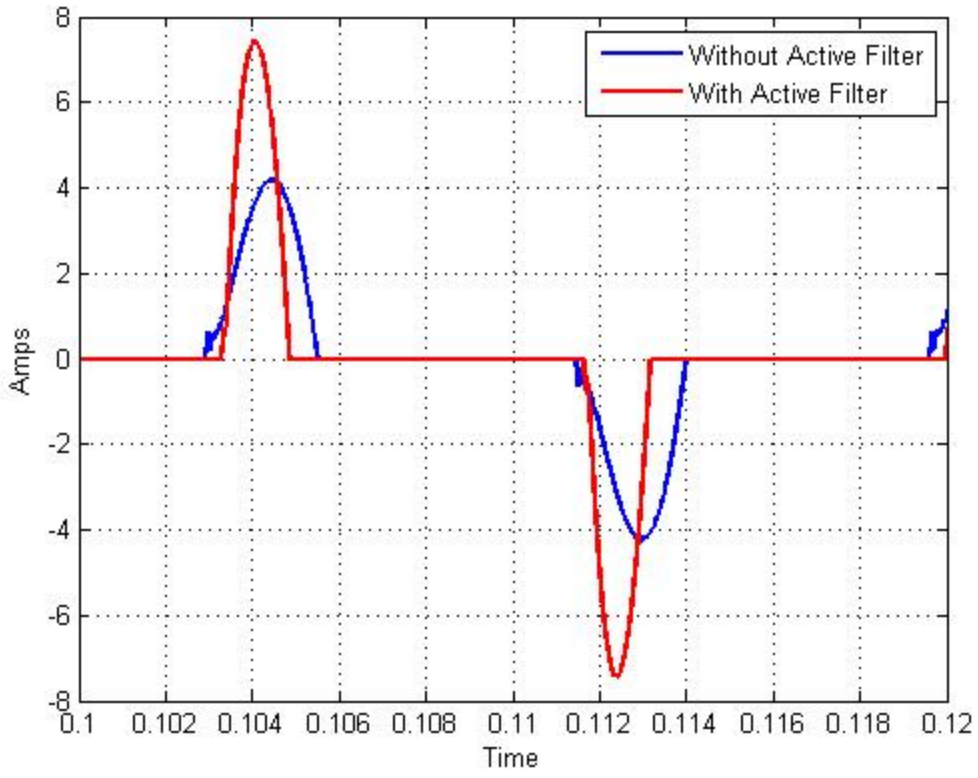

Figure 36. Active filter results on a passive diode rectifier.

B. FUTURE WORK AND RECOMMENDATIONS

MIL-STD-1399-300B has much tighter specifications on loads than it does on power sources. This was evident in the evaluation of the linear load connected to the EMS. The resistive linear load is near ideal, yet out-of-specification line current harmonics were still evident. This demonstrated that a VSI providing an output voltage well within specification was not clean enough to supply a linear load. Passive methods to remedy this may be to increase the switching frequency and/or increase the output filter.

It also appears that specifications are slowly being updated to account for newer technology. As ship power and industry move to renewable or DC energy systems, VSIs will be part of this technological step. A power source that is within specifications should be able to supply power to an ideal source (linear load) while maintaining line currents within specification. A review of VSIs as a power source compared to existing specifications is warranted.

The Simulink model used was mostly ideal with some factors taken into account like the 2.5 V 120 Hz loading pulsation found on the DC bus supplying the H-bridge. Further modeling of individual components such as the diodes and IGBTs can be worked into the model to achieve a higher accuracy. Furthermore, with research showing that active filtering as a non-ideal method in correcting distortion for a diode rectifier load, the use of a power factor correction (PFC) converter may be the answer to control distortion in the EMS. A bridgeless pseudo-boost PFC converter is analyzed in [8] but does not evaluate the THD. Modeling this converter, to include lab verification, would be the next recommended step in evaluating the islanding mode of the EMS.

THIS PAGE INTENTIONALLY LEFT BLANK

APPENDIX–MATLAB CODE

```
% LT Andrew Metzcus
%   H-bridge Inverter analysis from an Energy Management System (EMS).
%
% This file accomplishes the follwing:
% Acuisition of exported data from the oscilloscope connected to the
EMS,
%   and plots it versus time.
% This file requires the Hbridge_AnalysisModel.mdl to be ran first as
it:
%   anyalyzes the simulation results and compares it to that of the
%   physical data exported from the oscilloscope.
%%%%%%%%%%%%%%%%%%%%%%%%%%%%%%%%%%%%%%%%%%%%%%%%%%%%%%%%%%%%%%%%%%%%%%%
%%
%
%    DIODE LOAD
%
%
%%%%%%%%%%%%%%%%%%%%%%%%%%%%%%%%%%%%%%%%%%%%%%%%%%%%%%%%%%%%%%%%%%%%%%%
%%
data_xls=xlsread('Tek_CH1_Wfm.csv');
len = length(data_xls);
data=data_xls(15:len,1:2);
newlen=length(data); %this equals 10,000 rows col_1-time col_2-vout
time_vec=data(:,1);  %column 1 only from xls - time
data_vec=data(:,2);  %column 2 only from xls - vout
time_vec=time_vec+.0677;

Fs=250e3; %sampling frequency from oscope
T=.01647;
len2=round(Fs*T);
k=0:len2-1;
freq=k/T;

freqDomain=fft(data_vec(1:len2))/len2;
Vrms_freqDomain= 2*abs(freqDomain(1:len2)/sqrt(2));

figure(1);
plot(time_vec,data_vec,'LineWidth',2);
title('Data set from Scope: Output voltage - Diode Rectifier Load');
xlabel('Time'); ylabel('Volts');
axis([.065 .092 -150 150]);
grid on

figure(2)
IHDlimit=0.03*Vrms_freqDomain(2); %MilStd limit for IHD is 3%
loglog(freq(2:len2),Vrms_freqDomain(2:len2),'bo',freq(3:len2),IHDlimit,
'kx','LineWidth',2);
axis([50 40000 .01 200])
xlabel('Freq (Hz)');ylabel('Amplitude - Vrms');
title('Harmonics with Diode Rectifier Load');
legend('Individual Harmonic levels','3% MilStd limit');
```

```
grid on

% %THD calculation
THDdata=Vrms_freqDomain(3:30); %2nd through 29th harmonic --(1) is DC
(2) is 60Hz
THDsquare=THDdata.*THDdata;
THDsum=sum(THDsquare);
THD=sqrt(THDsum)/Vrms_freqDomain(2)

figure(3)
idata_xls=xlsread('Tek_CH3_Wfm.csv');
ilen = length(idata_xls);
idata=idata_xls(15:ilen,1:2);
inewlen=length(idata); %this equals 10,000 rows col_1-time col_2-vout
itime_vec=idata(:,1);  %column 1 only from xls - time
idata_vec=idata(:,2);  %column 2 only from xls - load current
itime_vec=itime_vec+.0677;
plot(itime_vec,idata_vec,'LineWidth',2);
title('Load Current - Is');
xlabel('Time'); ylabel('Amps');
axis([.065 .092 -5 5]);
grid on

% %THD calculation- Current
ifreqDomain=fft(idata_vec(1:len2))/len2;
Irms_freqDomain= 2*abs(ifreqDomain(1:len2)/sqrt(2));

iTHDdata=Irms_freqDomain(3:30); %2nd through 29th harmonic --(1) is DC
(2) is 60Hz
iTHDsquare=iTHDdata.*iTHDdata;
iTHDsum=sum(iTHDsquare);
iTHD=sqrt(iTHDsum)/Irms_freqDomain(2)

figure(4);
plot(time_vec,data_vec,'LineWidth',2);
title('Output voltage Comparison');
xlabel('Time'); ylabel('Volts');
axis([.065 .092 -150 150]);
grid on
hold on
plot(time, Vcap, 'r','LineWidth',2);
legend('Laboratory','Model');

figure(5)
plot(itime_vec,idata_vec,'LineWidth',2);
title('Load Current Comparison');
xlabel('Time'); ylabel('Amps');
axis([.065 .092 -5 5]);
grid on
hold on
plot(time, is, 'r','LineWidth',2);
legend('Laboratory','Model');

simFs=1/20/tstep; %sampling frequency from simulation
```

```
simlen2=round(1/60*simFs); %obtains number of samples in one cycle
simk=0:simlen2-1;       %create a vector from 0 to newlen-1
simT=simlen2/simFs;        %get the frequency interval
simfreq=simk/simT;         %create the frequency range

figure(6);
plot(time,Vcap, 'r','LineWidth',2);
title('Simulation Results: Vcap with Diode Rectifier Load');
xlabel('Time'); ylabel('Volts');
axis([.065 .092 -150 150]);
grid on

figure(7)
plot(time, is, 'r','LineWidth',2);
axis([.07 .1 -5 5]);
title('Simulation Results: Load Current - Is');
xlabel('Time'); ylabel('Amps');
axis([.065 .092 -5 5]);
grid on

simfreqDomain=fft(Vcap((4*simlen2):(5*simlen2)))/simlen2; %fft of 4th
cycle of simulation
simVrms_freqDomain= 2*abs(simfreqDomain(1:simlen2)/sqrt(2));

THDsimdata=simVrms_freqDomain(3:30); %2nd through 29th harmonic --(1)
is DC (2) is 60Hz
THDsimsquare=THDsimdata.*THDsimdata;
THDsimsum=sum(THDsimsquare);
THDsim=sqrt(THDsimsum)/simVrms_freqDomain(2)

figure(8)
simIHDlimit=0.03*simVrms_freqDomain(2); %MilStd limit for IHD is 3%
loglog(freq(2:len2),Vrms_freqDomain(2:len2),'b','linewidth',2);
%Labratory
hold on
loglog(simfreq(2:simlen2),simVrms_freqDomain(2:simlen2),'r','linewidth'
,2);%sim Unipolar
loglog(simfreq(3:simlen2),simIHDlimit,'k*','LineWidth',2); % "3%" MIL-
STD-1399-300A limit
title('Voltage Harmonic Comparison');
axis([50 10000 .0001 200])
xlabel('Freq (Hz)');ylabel('Amplitude - Vrms');
title('Voltage Harmonic Comparison');
legend('Laboratory','Model','3% MilStd limit');
grid on
hold off

sz=size(freq);
freq1=ones(sz);
freq1=6000.*freq1;
freqlimit=freq1./freq;

Irms_freq_percent=Irms_freqDomain./Irms_freqDomain(2).*100;
```

```
isimfreqDomain=fft(is((4*simlen2):(5*simlen2)))/simlen2; %fft of 4th
cycle of simulation
simIrms_freqDomain= 2*abs(isimfreqDomain(1:simlen2)/sqrt(2));
simIrms_freq_percent=simIrms_freqDomain./simIrms_freqDomain(2).*100;

iTHDsimdata=simIrms_freqDomain(3:30); %2nd through 29th harmonic --(1)
is DC (2) is 60Hz
iTHDsimsquare=iTHDsimdata.*iTHDsimdata;
iTHDsimsum=sum(iTHDsimsquare);
iTHDsim=sqrt(iTHDsimsum)/simIrms_freqDomain(2);

figure(10)
semilogx(freq(3:len2),Irms_freq_percent(3:len2),'bo','linewidth',2);
%Labratory
grid on
hold on
semilogx(simfreq(3:len2),simIrms_freq_percent(3:len2),'rd','linewidth',
2);
semilogx(simfreq(2:len2),freqlimit(2:len2),'k','LineWidth',2); %MIL-
STD-1399-300B limit
title('Harmonic Line Current Comparison with diode rectifier load');
axis([10 20000 0 100])
xlabel('Freq (Hz)');ylabel('% of 60Hz Fundamental Current (A)');
legend('Laboratory','Model',sprintf('MilStd limit: 60Hz user\n
equipment <1kVA'));
grid on
hold off

%%%%%%%%%%%%%%%%%%%%%%%%%%%%%%%%%%%%%%%%%%%%%%%%%%%%%%%%%%%%%%%%%%%%%%%
%%%%%%%%%%%%%%%%
%Code Below is for showing how unipolar has the effect of doubling the
%switching frequency
%%%%%%%%%%%%%%%%%%%%%%%%%%%%%%%%%%%%%%%%%%%%%%%%%%%%%%%%%%%%%%%%%%%%%%%
%%%%%%%%%%%%%%%%
% figure(11)
%
loglog(simfreq(2:simlen2),simVrms_freqDomain(2:simlen2),'b','linewidth'
,6);%sim Unipolar
% hold on
%
loglog(simfreq(2:simlen2),simVrms_freqDomainbi(2:simlen2),'r','linewidt
h',2);%sim Bipolar
% loglog(simfreq(3:simlen2),simIHDlimit,'k*'); % "3%" MIL-STD-1399-300A
limit
% title('Unipolar vs Bipolar Simulation Comparison - Voltage
Harmonics');
% legend('Unipolar','Bipolar','3% MilStd limit');
% axis([50 40000 .0001 200])
% xlabel('Freq (Hz)');ylabel('Amplitude - Vrms');
% grid on
% hold off

%%%%%%%%%%%%%%%%%%%%%%%%%%%%%%%%%%%%%%%%%%%%%%%%%%%%%%%%%%%%%%%%%%%%%%%
%%%%%%%%%%%%%%
%
```

```
%  The Code Below is for the analysis of the Linear Load
%
%%%%%%%%%%%%%%%%%%%%%%%%%%%%%%%%%%%%%%%%%%%%%%%%%%%%%%%%%%%%%%%%%%%%%%%
%%%%%%%%%%%%%%

data_xls=xlsread('Tek_CH1_Wfm_linear.csv');
len = length(data_xls);
data=data_xls(15:len,1:2);
newlen=length(data); %this equals 10,000 rows col_1-time col_2-vout
time_vec=data(:,1);  %column 1 only from xls - time
data_vec=data(:,2);  %column 2 only from xls - vout
time_vec=time_vec+.0677;

Fs=250e3; %sampling frequency from oscope
T=.01647;
len2=round(Fs*T);
k=0:len2-1;
freq=k/T;

freqDomain=fft(data_vec(1:len2))/len2;
Vrms_freqDomain= 2*abs(freqDomain(1:len2)/sqrt(2));

figure(12)
idata_xls=xlsread('Tek_CH3_Wfm_linear.csv');
ilen = length(idata_xls);
idata=idata_xls(15:ilen,1:2);
inewlen=length(idata); %this equals 10,000 rows col_1-time col_2-vout
itime_vec=idata(:,1);  %column 1 only from xls - time
idata_vec=idata(:,2);  %column 2 only from xls - load current
itime_vec=itime_vec+.0677;
plot(itime_vec,idata_vec,'LineWidth',2);
title('Load Current - Is');
xlabel('Time'); ylabel('Amps');
axis([.065 .092 -5 5]);
grid on

% %THD calculation- Current
ifreqDomain=fft(idata_vec(1:len2))/len2;
Irms_freqDomain= 2*abs(ifreqDomain(1:len2)/sqrt(2));

iTHDdata=Irms_freqDomain(3:30); %2nd through 29th harmonic --(1) is DC
(2) is 60Hz
iTHDsquare=iTHDdata.*iTHDdata;
iTHDsum=sum(iTHDsquare);
iTHD=sqrt(iTHDsum)/Irms_freqDomain(2)

figure(13);
plot(time_vec,data_vec,'LineWidth',2);
title('Output voltage - Linear Load');
xlabel('Time'); ylabel('Volts');
axis([.065 .092 -150 150]);
grid on

figure(14)
```

```
IHDlimit=0.03*Vrms_freqDomain(2); %MilStd limit for IHD is 3%
loglog(freq(2:len2),Vrms_freqDomain(2:len2),'bo',freq(3:len2),IHDlimit,
'kx','LineWidth',2);
axis([50 20000 .01 200])
xlabel('Freq (Hz)');ylabel('Amplitude - Vrms');
title('Harmonics with Linear Load');
legend('Individual Harmonic levels','3% MilStd limit');
grid on

% %THD calculation
THDdata=Vrms_freqDomain(3:30); %2nd through 29th harmonic --(1) is DC
(2) is 60Hz
THDsquare=THDdata.*THDdata;
THDsum=sum(THDsquare);
THD=sqrt(THDsum)/Vrms_freqDomain(2)

figure(15)
idata_xls=xlsread('Tek_CH3_Wfm_linear.csv');
ilen = length(idata_xls);
idata=idata_xls(15:ilen,1:2);
inewlen=length(idata); %this equals 10,000 rows col_1-time col_2-vout
itime_vec=idata(:,1);  %column 1 only from xls - time
idata_vec=idata(:,2);  %column 2 only from xls - load current
itime_vec=itime_vec+.0677;
plot(itime_vec,idata_vec,'LineWidth',2);
title('Load Current with Linear Load');
xlabel('Time'); ylabel('Amps');
axis([.065 .092 -1 1]);
grid on

figure(16);
plot(time_vec,data_vec,'LineWidth',2);
title('Output voltage Comparison with Linear Load');
xlabel('Time'); ylabel('Volts');
axis([.065 .092 -150 150]);
grid on
hold on
plot(time, Vcap_linear, 'r','LineWidth',2);
legend('Laboratory','Model');

figure(17)
plot(itime_vec,idata_vec,'LineWidth',2);
hold on
plot(time, Is_linear, 'r','LineWidth',2);
title('Load Current Comparison with Linear Load');
xlabel('Time'); ylabel('Amps');
axis([.065 .092 -1 1]);
grid on
legend('Laboratory','Model');
hold off

simFs=1/20/tstep; %sampling frequency from simulation
simlen2=round(1/60*simFs); %obtains number of samples in one cycle
simk=0:simlen2-1;       %create a vector from 0 to newlen-1
```

```
simT=simlen2/simFs;        %get the frequency interval
simfreq=simk/simT;         %create the frequency range

figure(18);
plot(time,Vcap_linear, 'r','LineWidth',2);
title('Simulation Results: Vcap with Linear Load');
xlabel('Time'); ylabel('Volts');
axis([.065 .092 -150 150]);
grid on

figure(19)
plot(time, Is_linear, 'r','LineWidth',2);
axis([.07 .1 -5 5]);
title('Simulation Results: Load Current with Linear Load');
xlabel('Time'); ylabel('Amps');
axis([.065 .092 -1 1]);
grid on

simfreqDomain=fft(Vcap_linear((4*simlen2):(5*simlen2)))/simlen2; %fft
of 4th cycle of simulation
simVrms_freqDomain= 2*abs(simfreqDomain(1:simlen2)/sqrt(2));

THDsimdata=simVrms_freqDomain(3:30); %2nd through 29th harmonic --(1)
is DC (2) is 60Hz
THDsimsquare=THDsimdata.*THDsimdata;
THDsimsum=sum(THDsimsquare);
THDsim=sqrt(THDsimsum)/simVrms_freqDomain(2)

figure(20)
simIHDlimit=0.03*simVrms_freqDomain(2); %MilStd limit for IHD is 3%
loglog(freq(2:len2),Vrms_freqDomain(2:len2),'b','LineWidth',2);
hold on
loglog(simfreq(2:simlen2),simVrms_freqDomain(2:simlen2),'r','LineWidth'
,2);
loglog(simfreq(3:simlen2),simIHDlimit,'k*','LineWidth',2);
axis([50 10000 .0001 200])
xlabel('Freq (Hz)');ylabel('Amplitude - Vrms');
title('Voltage Harmonic Comparison with Linear Load');
legend('Laboratory','Model','3% MilStd limit');
grid on
hold off

sz=size(freq);
freq1=ones(sz);
freq1=6000.*freq1;
freqlimit=freq1./freq;

Irms_freq_percent=Irms_freqDomain./Irms_freqDomain(2).*100;

isimfreqDomain=fft(Is_linear((4*simlen2):(5*simlen2)))/simlen2; %fft of
4th cycle of simulation
simIrms_freqDomain= 2*abs(isimfreqDomain(1:simlen2)/sqrt(2));
simIrms_freq_percent=simIrms_freqDomain./simIrms_freqDomain(2).*100;
```

```
iTHDsimdata=simIrms_freqDomain(3:30); %2nd through 29th harmonic --(1)
is DC (2) is 60Hz
iTHDsimsquare=iTHDsimdata.*iTHDsimdata;
iTHDsimsum=sum(iTHDsimsquare);
iTHDsim=sqrt(iTHDsimsum)/simIrms_freqDomain(2);

figure(21)
semilogx(freq(3:len2),Irms_freq_percent(3:len2),'bo','linewidth',2);
%Laboratory
grid on
hold on
semilogx(simfreq(3:len2),simIrms_freq_percent(3:len2),'rd','linewidth',
2);
simIrms_freq_percent_orig=simIrms_freq_percent;
semilogx(simfreq(2:len2),freqlimit(2:len2),'k','LineWidth',2); %MIL-
STD-1399-300B limit
title('Harmonic Line Current Comparison with Linear Load');
axis([10 20000 0 10])
xlabel('Freq (Hz)');ylabel('% of 60Hz Fundamental Current (A)');
legend('Laboratory','Model',sprintf('MilStd limit: 60Hz user\n
equipment <1kVA'));
grid on
hold off

figure(22)
[haxes,hline1,hline2] = plotyy(time,Vcap,time,is);

axes(haxes(1))
 axis([.065 .092 -160 160])
 ylabel('Volts');
 set(hline1,'Color','b','LineWidth',2)
 grid on
axes(haxes(2))
 set(hline2,'Color','r','LineWidth',2)
 axis([.065 .092 -8 8])
 ylabel('Amps');
 xlabel('Time');
 grid on
 legend('Current','Voltage');
set(haxes,{'ycolor'},{'b';'r'})
title('Simulated Voltage and Current w/o Active Filter')

figure(23)
[haxes,hline1,hline2] = plotyy(time,Vcap_active,time,is_active);
axes(haxes(1))

 axis([.065 .092 -160 160])
 ylabel('Volts');
 set(hline1,'Color','b','LineWidth',2)
 grid on
 set(gca,'YTick',[-150 -100 -50 0 50 100 150])

axes(haxes(2))
 set(hline2,'Color','r','LineWidth',2)
```

```
 axis([.065 .092 -8 8])
 ylabel('Amps');
 xlabel('Time');
 grid on
 legend('Current','Voltage');
 set(gca,'YTick',[-6 -4 -2 0 2 4 6])
set(haxes,{'ycolor'},{'b';'r'})
title('Simulated Voltage and Current w/ Active Filter')
```

THIS PAGE INTENTIONALLY LEFT BLANK

LIST OF REFERENCES

[1] Office of Naval Research. (2009 October). *Naval energy–A strategic approach* [Online]. Available: http://www.onr.navy.mil/naval-energy-forum/~/media/Files/Conferences/Naval%20Energy%20Forum/Naval%20Energy%20Strategy%20overview.ashx

[2] Shore Energy Management, OPNAVINST 4100.5E, June 22, 2012.

[3] G. Oriti, A. L. Julian, and N.J. Peck, "Power electronics enabled energy management systems," in *Proc. of IEEE Applied Power Electronics Conf. (APEC)*, Long Beach, CA, Mar., 2013.

[4] F.Z. Peng, Y.W. Li, and L.M. Tolbert, "Control and protection of power electronics interfaced distributed generation systems in a customer-driven microgrid," in *Proc. of IEEE Power and Energy Society General Meeting*, Calgary, AB, Canada, pp. 1–8, July 2009.

[5] Wikipedia, s.v. "Field programmable gate arrays," last modified May 21, 2013, http://en.wikipedia.org/wiki/FPGA [Accessed: June 3, 2013].

[6] N. Mohan and T. Undeland, W. P. Robbins, Power Electronics, Converters Applications and Design, (3rd edition), New York: John Wiley and Sons, 2003.

[7] J.G. Pinto, P. Neves, R. Pregitzer, L. F. C. Monteiro, and J L. Afonso, "Single-phase shunt active filter with digital control," at *International Conference on Renewable Energies and Power Quality (ICREPQ'07),* Seville, Spain, March 2007.

[8] Z. Chen, J. Xu, F. Zhang, "Analysis of bridgeless pseudo-boost PFC converter," in *Proc. of IEEE International Symposium on Industrial Electronics,* Hangzhou, China, pp. 189–193, May 2012

[9] DOD Interface Standard Section 300B Electric Power, Alternating Current, MIL-STD-1399-300B, April 24, 2008.

THIS PAGE INTENTIONALLY LEFT BLANK

INITIAL DISTRIBUTION LIST

1. Defense Technical Information Center
   Ft. Belvoir, Virginia

2. Dudley Knox Library
   Naval Postgraduate School
   Monterey, California